CHARACTERISING GROUNDWATER–SURFACE WATER EXCHANGE IN THE WAIKIRIKIRI SELWYN RIVER, USING RADON

A thesis submitted in partial fulfilment of the requirements for the Degree of Master of Water Resource Management in the Waterways Centre for Freshwater Management

By Linda Robb

University of Canterbury

2021

Abstract

Quantifying groundwater–surface water interactions in braided rivers has considerable uncertainties, due to the dynamic nature of the river system and the heterogeneity of the sediments. The ability to quantify recharge rates to groundwater from these complex systems is of vital importance for freshwater management. Environmental tracers such as radon have proven to be useful tools to aid in characterising groundwater–surface water interactions in other settings. This research investigates the spatial variability of radon equilibrium concentrations in the braid plain sediments of the upper Waikirikiri Selwyn River, Canterbury, New Zealand. This is important because previous studies have assumed the radon concentration within the sediments is evenly distributed.

Sediments were collected during the drilling of monitoring wells in the braid plain of the Waikirikiri Selwyn River. These monitoring wells were drilled through two geological formations, the Springston Formation (0–6 m) and the Burnham Formation (6-16 m). Grain size analysis was carried out on 32 sediment samples. Following this, 318 radon equilibrium experiments were carried out on samples from across the study site. Grain size fractions from one of the installed piezometers, Selwyn 5, were also used in the radon experiments.

Analysis of sediment cores revealed a heterogeneous structure. The grain size analysis presented relatively consistent distribution curves showing a large range in grain size fractions. Hydraulic conductivity values were estimated from the grain sizes using a number of empirical formula and were found to vary vertically and spatially depending on the percentage of core recovery and formula used. The values ranged from ~ 80– >1,000 m/d. The calculated porosity ranged from 0.18 to 0.3 and bulk density values ranged from 1400 kg/m^3 to 1700 kg/m^3 and were similar to studies within the same region.

Radon equilibrium concentrations of water samples were tested after the water had been in a sealed jar with the sediments for 30 days, until secular equilibrium was reached. It was evident from the 318 samples analysed that radon concentration varied with differing grain size. Specifically, the <63 µm fraction contained significantly more radon than the other grain size fractions sampled. When comparing the spatial variability with the Springston and Burnham formations it appears that the radon concentration increases with depth within both these formations.

This study has provided baseline data within the research site on the radon equilibrium concentrations both spatially and within differing grain size fractions. The results suggest that radon concentrations in groundwater depend on the volume of silts and clays in the subsurface. Therefore, using radon as a tracer for groundwater–surface water interactions may be more complex than first thought.

Acknowledgements

Firstly, I would like to thank my supervisory team of, Leanne Morgan, Eddie Banks and Scott Wilson for their support and guidance throughout my thesis. I am very grateful for your patience with my writing, answering queries and catching up as required.

Thanks to all the technical staff, in particular John Revell for the experimental set-up and my continued queries and Chris Grimshaw for teaching me all my sediment knowledge. I now know a lot about sediments! Thanks to Suellen from the Waterways department for all your guidance with my never-ending queries!

I would also like to thank the Waterways Centre for Freshwater Management for their scholarship as this made completing my masters slightly less stressful.

Finally, thanks to my partner, Paul and my three children who have endured my frustrations and grumpiness when things did not go to plan! Paul, my mental health coach when I lacked self-belief.

Table of Contents

List of Figures

List of Tables

Glossary

Alluvial River – a river where the banks and bed of the river are made up of moveable sediment.

Bulk density – the weight of rock divided by the total volume of the rock.

Braided river – a river consisting of many channels separated by bars/ islands. They generally have a gravel bed.

Braid plain – the area a braided river moves across and has previously occupied.

Geomorphology – the study of the landscape.

Grain size distribution – the distribution of grain sizes for a particular sediment sample.

Groundwater – the water contained below the water table in either a confined or unconfined aquifer.

Heterogeneity – physical properties are different in different locations.

Hydraulic conductivity – the ease with which water moves through a porous medium**.** It is dependent upon the fluid properties and the properties of the medium it is passing through.

Porosity – the percentage of rock or soil that is void of material.

Radon – a soluble, noble gas of half-life 3.82 days.

Radon emanation – when a material containing radium allows an atom of radon to escape into the pore space.

1 Introduction

Globally, groundwater systems are under pressure due to climate change and water abstraction for irrigation and human activities (Treidel et al., 2012). These pressures will impact upon groundwater quantity and quality (Gurdak et al., 2012). Climate change is increasing temperatures and changing precipitation patterns, affecting recharge rates of groundwater and the height of the water table (Bovolo et al., 2009). Therefore, there is a need for more accurate information on which to base water allocation decisions. Increasing our knowledge of how groundwater and surface water are integrated will allow water resources to be managed more effectively (Stellato et al., 2013).

Many rivers in New Zealand recharge the underlying aquifer system, assisting with groundwater storage and sustaining spring flows (White, 2001). However, in braided rivers, estimates of river–aquifer fluxes have considerable uncertainties, due to their dynamic nature (Close et al., 2014). A braided river is characterised by having many moving channels interwoven with gravel islands and bars across a braid plain. Braided rivers, much like alluvial rivers, have flow patterns that can vary both spatially and temporally due to inflow rates, groundwater–surface water exchange and channel planform. An alluvial river is a river that has boundaries formed by sediment that has been deposited previously or a river which has banks consisting of mobile sediment and are self-formed (Wang et al., 2015). Most braided rivers are alluvial rivers. The mobility of braided rivers creates complexities for water managers to forecast river flow rates, estimate flow from river stage height records, and, determine groundwater recharge rates (Rupp et al., 2008).

A promising approach for characterising groundwater–surface water exchange involves environmental tracers such as radon (Bourke et al., 2014; Lamontagne & Cook, 2007; Sadat-

Noori & Glamore, 2019). Radon is abundant in groundwater but degasses quickly with air contact, resulting in negligible amounts in surface water (Close et al., 2014; Stellato et al., 2008). In certain rock types and mineralogy, surface water that becomes groundwater will accumulate radon along its flow path through the subsurface. This property can be used to estimate losses of surface water to groundwater. However, before we estimate these losses, it is important to understand the background variability of radon in the subsurface. The focus of this research involves determining the spatial variability in radon equilibrium concentrations in an alluvial deposit adjacent to a braided river, the Waikirikiri Selwyn.

1.1 Groundwater–Surface Water Interaction in Braided Rivers

To sustainably manage water resources and ecosystems in braided rivers it is critical to understand the exchange between groundwater and surface water (Cartwright & Hofmann, 2016; Cartwright et al., 2014; Kalbus et al., 2006). The main source of recharge for groundwater systems is water from rainfall and rivers, therefore, measuring both provides important information for surface water and groundwater allocations (White, 2001).

Surface and groundwater interactions can vary temporally and spatially due to a number of factors, such as changes in flow, hydraulic gradient, streambed material and physical characteristics. It is particularly difficult to characterise the groundwater–surface water exchange of a gravel bed braided river due to the heterogeneity of the subsurface, the changing flow, and the geomorphology of the river (Coluccio, 2018).

Limited research has been undertaken to understand the groundwater–surface water flow paths of braided rivers and their surrounding environments, as noted by Coluccio and Morgan (2019). These flow paths are affected by the heterogeneity of the deposition and geomorphology of braided rivers such as constant channel movement and changing margins

(Coluccio & Morgan, 2019). The heterogeneity of the substrate of braided rivers can make it difficult to interpret concurrent flow gauging data, as there can be many small interactions within river stretches that differential flow gauging cannot identify (Coluccio & Morgan, 2019).

1.2 Environmental Tracers for Estimating Losses to Groundwater from Braided Rivers

Environmental tracers can be used to show the flow paths between surface water and groundwater in braided rivers. There are a variety of different environmental tracers. These include electrical conductivity, stable isotopes such as ^{2}H and ^{18}O, and dissolved gases (e.g., chloroflurocarbons) and chloride. In addition alkalinity and radioactive isotopes including radon can also be used as environmental tracers (Coluccio & Morgan, 2019; Cook, 2013; Kalbus et al., 2006; McCallum et al., 2012; Rodgers et al., 2004). There have been several studies using radon to measure groundwater inflows to surface water (Cook et al., 2003; Cook et al., 2006; Stellato et al., 2008). However, there has been limited research using radon to study surface water losses to groundwater, specifically in braided rivers. This research seeks to address this gap.

1.3 Radon

Radioactive elements, including radon, occur naturally in all rocks and soils at differing concentrations. The uranium-238 decay series produces radon-222, which has a half-life of 3.82 days, making it a useful environmental tracer (Cecil & Green, 2000).

Radon is a radioactive noble soluble gas (Cecil & Green, 2000). Surface water has low concentrations of radon caused by the gas exchange with the air, but there is an abundance in groundwater (Cook et al., 2003; Cook et al., 2006). This difference makes it an excellent tracer to show groundwater–surface water interactions (Avery et al., 2018; Cook et al.,

2006; Hoehn & Von Gunten, 1989; Stellato et al., 2013). Radon has been used as a tracer in a variety of environmental investigations such as: groundwater–surface water exchange, groundwater flow paths, and groundwater recharge (Cecil & Green, 2000).

The concentration of radon in groundwater depends upon where the uranium and its decay product, radium-226, occur within the rock. For high radon concentrations in water, radium must be present near the surface of the rocks, allowing more radon to enter the water and be measurable (Cecil & Green, 2000; Martindale, 2015).

1.4 Previous Studies Using Radon in Braided Rivers

Coluccio and Morgan (2019) reviewed international braided river research including those studies that used radon as a tracer. Moore (1997) studied the Brahmaputra River in the Bay of Bengal and used radon to estimate groundwater inflows to the delta. Acuña and Tockner (2009) use radon to calculate the residence time of the upwelling groundwater in the hyporheic zone of the Tagliamento River in Italy, using radon. Their results showed that radon improved estimates of the groundwater residence time as opposed to using the diel temperature pulse along a flow path length, but also found that radon was limited to estimating residence times of hours or days.

Recent studies have been conducted on braided rivers in New Zealand using radon as a tracer (Close, 2014; Close et al., 2014; Martindale et al., 2016). Close et al. (2014) measured radon in nearby and surrounding wells of the Waimakariri River in Canterbury. As the distance from the river increased, the concentration of radon in the shallow wells increased. The radon data were used to calculate the groundwater velocity near the river and the radon equilibrium value. No recharge flux estimations were calculated with the radon data as the aquifer properties were not known at the study site. The study suggested that, over

time, recharge at a single location could be monitored using continuous radon measurements to show how recharge at that point varies with river flow and time. Estimations of the groundwater recharge can be determined from the calculated velocities, however, these are dependent upon the assumed aquifer properties and dimensions (Close et al., 2014).

Close (2014) sampled radon in the Wairau River, Marlborough and surrounding groundwater to gain information on the exchange of groundwater and surface water. This information was used to quantify recharge to the aquifer, and also to show the variability of the recharge. The radon measured indicated there was significant recharge to the aquifer from the river. However, the error increased at lower radon concentrations. It was noted that counting the radon concentration in samples for longer periods of time would reduce the error in the results. Both the Close et al., (2014) and Close (2014) studies assumed the radium distribution throughout the subsurface was homogeneous.

Martindale et al. (2016) studied the Hutt River and the Mangatainoka River in the Hutt valley in the North Island. The main aim of the research was to measure and map groundwater–surface water interactions. They found that flow gauging alone in a gravel-bed braided river was insufficient. The measurements showed that radon was useful for mapping groundwater discharge into the rivers. However, for more accurate results the combination of flow gauging and radon measurements gave more precise information on groundwater–surface water exchange, as flow gauging alone is insufficient due to the dynamic nature of braided rivers.

1.5 Radon Equilibrium Concentrations

In order to quantify groundwater–surface water interaction using radon, the equilibrium (or end-member) concentration of radon in the groundwater is required. The equilibrium concentration is generally determined using values measured in groundwater at a distance away from the river where it is assumed radon decay and growth are in equilibrium. However, radon concentrations can vary spatially and with different rock types (Cecil & Green, 2000). Radon emanation occurs when a material containing radium allows an atom of radon to escape into the pore space (Sakoda et al., 2011), as shown in Figure 1. The amount of radon emanating depends on how much radium is contained in the rocks and how much pore space there is through which the radon can escape. The configuration and density of the material will determine how far the radon atom can travel. Grain size is one of the factors that has been shown to affect the radon emanation rates (Chanyotha et al., 2014; Sakoda et al., 2011). The emanation process is thought to be comprised of two parts: alpha recoil, and diffusion. Alpha recoil is when the energy of the decay of an alpha particle moves the radioactive particle, in this case radon, from its initial position (Sun & Semkow, 1998). Nazaroff (1992) stated that the escape of radon from grains via diffusion into the pore space was negligible. Various vessels have been used for emanation experiments, as shown in Appendix B.

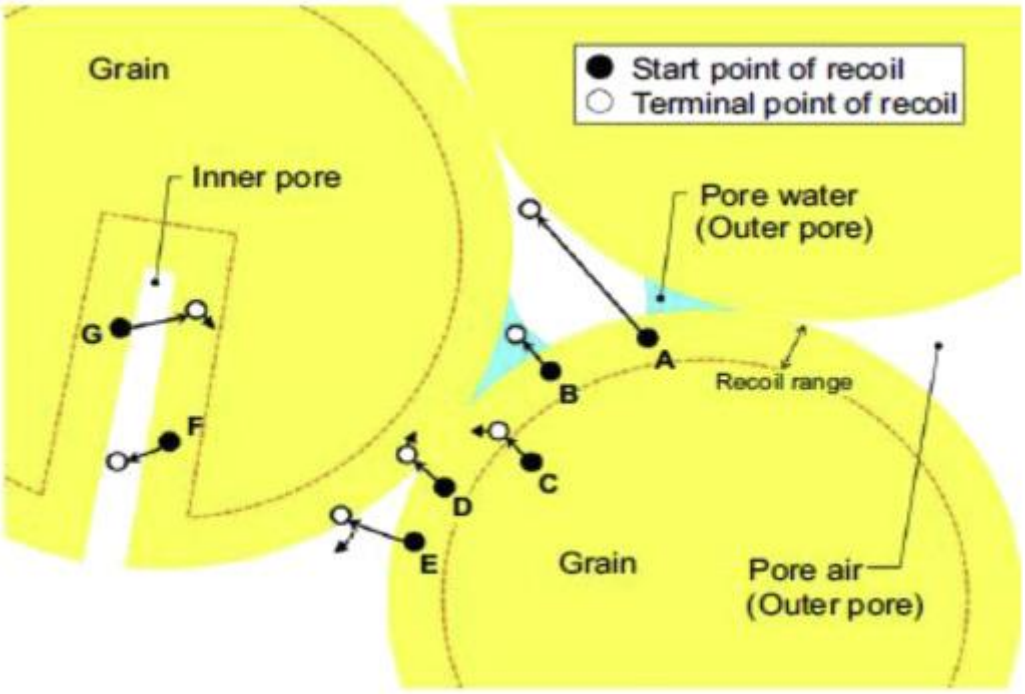

Figure 1 Scheme of radon emanation phenomenon.

Emanation occurs from atoms (A), (B), (E) and (F). No emanation occurs from atoms (C), (D) and (G). If radon cannot diffuse out from the inner pore space into the outer pore space, radon in point (F) should not be regarded as being emanated. Arrows following terminal points of recoil represent diffusion process, which are not to scale (Sakoda et al., 2011).

1.6 Case Study Site: The Waikirikiri Selwyn River

The location of the study site is the Waikirikiri Selwyn River on the South Island of New Zealand. It is one of three field sites of a 2020-2024 New Zealand Government-funded Ministry of Business, Innovation and Employment (MBIE) research project: 'Subsurface processes in braided rivers – hyporheic exchange and subsurface leakage to groundwater'. The two other field sites are the Wairau River, in Marlborough, and the Ngauroro River, in

the Hawkes Bay. One of the main aims of this research project is to quantify seepage rates from these rivers to the underlying aquifers.

The Waikirikiri Selwyn River is a gravel-bed braided river, beginning in the foothills of the Southern Alps. It flows through the Canterbury Plains and into a coastal lagoon, Te Waihora. The river is approximately 93 km in length (Larned et al., 2008) and has a catchment area of 974 km^2 (Rupp et al., 2008). The intermittency and flow of the river is regulated by groundwater seepage and surface run-off (Larned et al., 2008). Regional groundwater has been shown to flow from northwest to southeast, running parallel to the Waikirikiri Selwyn River (Larned et al., 2008; Vincent, 2005).

The Waikirikiri Selwyn River has three main tributaries: the Hororata, Wainiwaniwa and the Hawkins (Figure 2). All of these rivers drain their catchments in the foothills, but lose most of their water to the underlying aquifer (Larned et al., 2008). The Waikirikiri Selwyn River is an extremely complex river, where flow patterns vary temporally and spatially and with various states of connectivity (Larned et al., 2008).

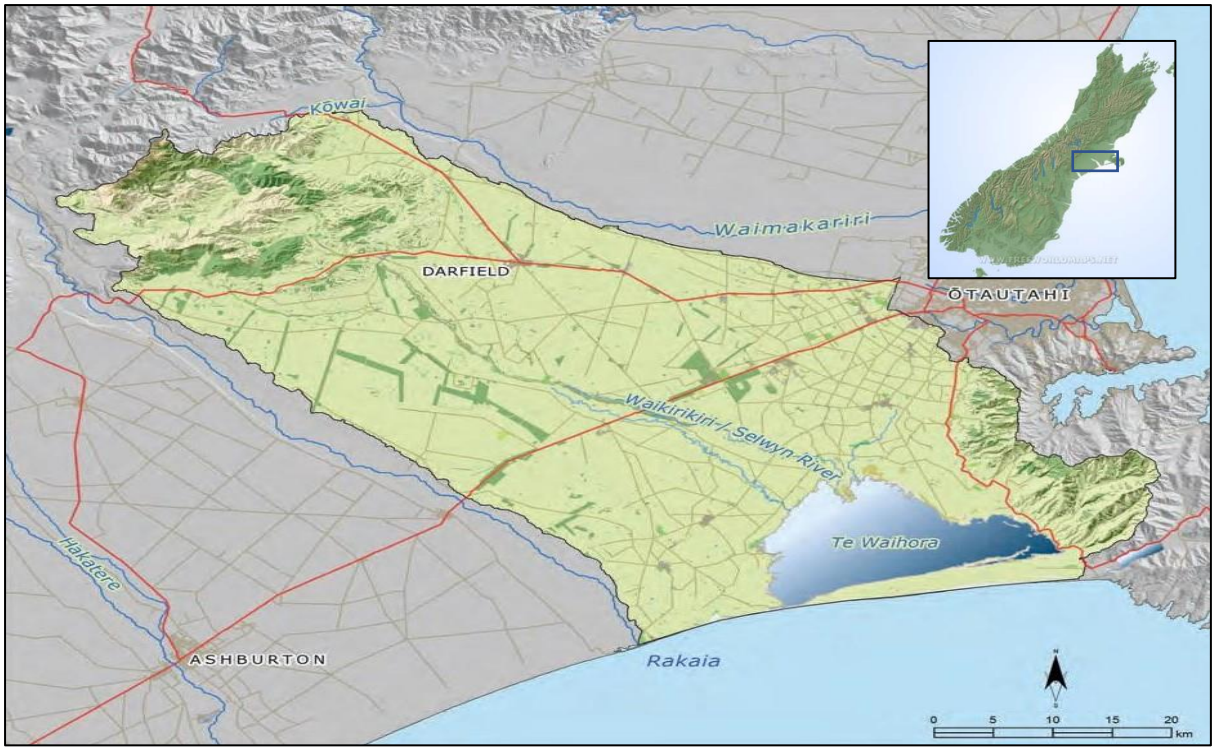

Figure 2 The Waikirikiri Selwyn River catchment

(Image source: https://mahaanuikurataiao.co.nz/iwi-management-plan/wahi-tuano/te-waihora/).

Throughout the upper Waikirikiri Selwyn catchment there are a variety of land uses such as sheep, beef, dairy, crops, deer, pigs and horticulture. Due to the availability of water and financial returns there has been an increase in irrigated agriculture and land development (Larned et al., 2008). Many farmers use groundwater or surface water from the Central Plains Water Scheme for irrigation (D. Clark, personal communication, April 14th 2020). Therefore, it is important to understand the groundwater–surface water exchange process in order to understand the effect of abstraction on different components of the hydrological cycle.

1.7 Overview of Hydrogeology in the Waikirikiri Selwyn Catchment

The Waikirikiri Selwyn River begins in the foothills of the Canterbury Plains. In terms of geology, the foothills consist mainly of impermeable greywacke. This, along with the steep gradient of the hills, causes most of the rainfall to be run-off for streams. The coastal plains consist of post–glacial alluvium and marine deposits where the sediments consist of peats, muds and permeable sands. The inner plains are mostly derived from glacial outwash gravels (Wilson, 1973).

According to Vincent (2005), the historical movement of the Waikirikiri Selwyn River and its tributaries is likely to have formed a depositional pattern of intertwining channels. Such a dynamic depositional environment will produce sediments, which have a large variability in grain-size and permeability over a small area. This depositional variability will influence groundwater flow, with much of the flow occurring preferentially through paleo-channels.

Vincent (2005) noted the water level fluctuations in the shallow wells, in the immediate vicinity of the river, suggest the aquifer level is effected by the river flow. There were fewer water level fluctuations in the shallow wells as the distance from the river increased. The groundwater recharge relies heavily on the river volumes and its flow duration.

1.8 Waikirikiri Selwyn River Sediments

Sediments were extracted via sonic drilling at the study site in the Waikirikiri Selwyn River. Sonic drilling allows for the recovery of sediments, using a vibrating and rotating drill head (McLean, 2018). The recovery of the sediment allows for the hydraulic conductivity to be estimated via grain size analysis of the sediments in the lab. Sediment cores were recovered from piezometers 1, 3, 5, 7 and 9 shown in Figure 3. These piezometers were all drilled down to around 16 m depth. Sediment recovery varied within each drillhole, depending on

the abundance of cobbles which, when present, can block the passage of material from the drill head to the sampling barrel.

The piezometers at the study site were constructed with 50 mm diameter PVC pipes, with slotted screen lengths of 3 m for all wells. Sand was placed around the screen and bentonite clay was used above the screen to hold the pipe in place and prevent preferential flow down the drillhole anulus.

Figure 3 Map of of piezometers at the Waikirikiri Selwyn River study site (Scott, 2020).

Figure 4 shows an example of the recovered sediment cores, which were logged in drill core boxes. The detailed lithology of the drillholes is shown in Table 1. The sediment cores were

sampled in intervals of similar lithology and the percentage of recovery. For simplicity, the lithology was characterized as 20 unique intervals by Scott Wilson (hydrogeologist at Lincoln Agritech). The intervals are highlighted in the table by colour coding. These sample intervals were then used for the grain size analysis and the radon equilibrium concentration measurements.

Figure 4 Sediment core recovery from Selwyn 1 (depth: 2.57-15.8 m).

Photo taken by Linda Robb, 11am, March 2020.

Table 1 Lithology and depth intervals of recovered core sediments from drillholes at the Waikirikiri Selwyn River study site.

Every second sample interval is highlighted to show the different sample intervals.

Piezo	From	To	Recovery	Description
Selwyn 01	2.57	3.84	100	3 cycles of small to large pebbles in silt/clay matrix (fining up)
Selwyn 01	4.44	4.76	100	Small pebbles and grains in brown silty matrix
Selwyn 01	4.76	5.96	100	Solid silty clay with small angular pebble grains
Selwyn 01	8.4	8.9	35	Fine loose gravel in sandy matrix, occasional large clasts
Selwyn 01	10.52	11.1	100	Solid silty clay with fine angular pebble chips
Selwyn 01	13.2	13.56	60	Fine pebbles in silty clay matrix
Selwyn 01	15.08	15.80	100	Gravel in fine sand to silty-clay matrix
Selwyn 03	0.95	1.4	100	Fine rounded pebbles in solid grey fine sand-silt-clay matrix
Selwyn 03	5.6	5.96	80	Brown fine sand to silty clay with angular pebbles and cobbles
Selwyn 03	13.56	14.4		Fine to medium clean sand coarsening downwards to coarse sand
Selwyn 03	14.85	15.08	60	Pebbles and cobbles in a hard silty clay matrix
Selwyn 05	3	3.5	60	Coarse angular sand grit & small subangular pebbles in silty clay matrix. Coarsening down to medium-large pebbles with less matrix
Selwyn 05	3.5	3.9	100	Coarse sand grit & small subangular pebbles in silty-clay matrix, coarsening down
Selwyn 05	4.05	4.44	100	Coarse sand & small subrounded pebbles in silty clay matrix grading down to large pebbles in silty clay matrix
Selwyn 05	4.9	5.1	100	Coarse sand & small subrounded pebbles in silty clay matrix grading down to large pebbles in silty clay matrix
Selwyn 05	5.5	6.0	100	Coarse angular sand to fine pebbles in silty clay matrix
Selwyn 05	6	6.6	100	Silt & clay with fine coarse sand and small angular pebbles grading down to large pebbles
Selwyn 05	6.6	6.9	100	Silt & clay with fine coarse sand and small angular pebbles grading down to large pebbles
Selwyn 05	6.9	7.2	100	Silt & clay with fine coarse sand and small angular pebbles grading down to large pebbles
Selwyn 05	7.2	7.5	100	Silt & clay with fine coarse sand and small angular pebbles grading down to large pebbles

Piezo	From	To	Recovery	Description
Selwyn 05	7.8	8.4	100	Coarse angular sand in silty clay matrix
Selwyn 05	8.7	9	80	Coarse angular sand to small pebbles in silt & clay, possibly clast-supported
Selwyn 05	9.2	9.8	80	Coarse angular sand to small pebbles in silt & clay, possibly clast-supported
Selwyn 05	9.8	10.1	80	Coarse angular sand to small pebbles in silt & clay, possibly clast-supported
Selwyn 05	10.1	10.5	80	Coarse angular sand to small pebbles in silt & clay with occasional large pebbles/ cobbles, possibly clast-supported
Selwyn 05	14	14.4	60	Silty clay with medium to coarse angular sand & small subangular pebbles
Selwyn 05	14.4	15.0	60	Silty clay with medium to coarse angular sand & small subangular pebbles
Selwyn 07	12.5	13	80	Coarse sand to fine angular pebbles grading down to large pebbles/ small cobbles in brown silty clay matrix
Selwyn 07	13	13.5	80	Coarse sand to fine angular pebbles grading down to large pebbles/ small cobbles in brown silty clay matrix
Selwyn 09	1.5	2.0	70	Rounded grey pebbles & cobbles in fine grey to coarse sand matrix
Selwyn 09	6.87	7.5	100	Small to medium pebbles in coarse sand, probably clast-supported
Selwyn 09	8.4	9.0	50	Small to medium pebbles & pea gravel, some coarse, occasional cobles

1.9 Aims

This research aims to provide baseline data to support the use of radon as a tracer in groundwater–surface water exchange in a braided river system, the Waikirikiri Selwyn River, Christchurch New Zealand. Spatial variability of the radon activities within the saturated sediments will be determined by calculating the radon equilibrium concentrations of sediment samples collected during the installation of monitoring wells at the site. A relationship between the variation of lithology type, grain size and porosity will also be undertaken.

1.9.1 Objectives

1. Use sediment cores from bore logs to determine grain size characteristics and lithology of aquifer material in the Waikirikiri Selwyn River braid plain.
2. Evaluate the variation of radon concentrations across the differing lithology beneath the Waikirikiri Selwyn River and how the grain size distribution affects the radon concentration.
3. Evaluate the suitability of using radon as a tracer for quantifying groundwater recharge rates from the Waikirikiri Selwyn River.

2 Methods

2.1 Grain Size Analysis

The sediment cores were sieved for grain size analysis using sieves ranging in size from 63 µm to 31.5 mm. The fines (<63 µm) were analysed using a Micrometrics® Saturn Digisizer, enabling a full analysis of the sediments. As shown in Figure 4, some sections of core contained abundant amounts of silt and clay, hence wet sieving with deionized water was used to enable recovery of the fines.

The samples were sieved and grouped together as per the intervals in Table 1. The sieves were stacked as shown in Figure 5 and sediments were placed in the top sieve together with deionised water and agitated to separate the grains. The material retained in the catch pan was considered 'fines'. The granules from each sieve were dried in an oven at 60˚C, to ensure the chemistry of the clays was not destroyed (C. Grimshaw, personal communication, June 11th, 2020). Once dried, the samples were then weighed, giving the weight of each sample of the defined grain size range. From this we obtained the cumulative percentage of the total mass passing each sieve.

A digisizer was used to analyse the fines, and sediment grain sizes ranging from 0.6 µm to 2100 µm. It uses a combination of a charged-couple device containing 3 million detectors and a laser to calculate the particle size. The intensity of light scattered by the particles at various angles is measured by the detectors. The size, shape, refractive index and wavelength of the light from the particles influences the pattern made by the light. The angle distribution of the scattered light intensity is collected by the detectors and the particle size distribution is measured founded on the Mie theory (Micrometrics, 2012). The

fines are mixed with a small amount of deflocculant, sodium hexametaphosphate, and the digisizer produces a report showing the percentage of each grain size for the sample.

On completion of the grain size distribution, a data set for each sample consisting of the grain diameter and the corresponding percentage of the sample fines by weight was obtained. This data was plotted on a semi-logarithmic graph with grain diameter on the x-axis. Data plotted on particle size distribution curves were used to estimate the hydraulic conductivity of the material (Cheong et al., 2008; Freeze & Cherry, 1979; Odong, 2007).

Figure 5 Sieving of sediment samples in lab.

2.2 Estimating Hydraulic Conductivity

There are several empirical models that relate hydraulic conductivity to grain size of a sediment (Freeze & Cherry, 1979). Odong (2007) compared the effectiveness of various empirical models and concluded that the Kozeny-Carmen model was the most suitable for a wide variety of soil types. However, for a heterogeneous sample, the Beyer method offered the best approximation.

Following Odong (2007), the Slichter , Kozeny-Carmen and Beyer empirical models were used to calculate the hydraulic conductivity of the sieved samples. The Hazen model was considered, however, to satisfy the model the d_{10} had to lie between 0.1 and 3mm and the uniformity coefficient had to be less than 5. None of the grain size distribution curves returned these values for the Hazen model, therefore this model was not used in the results.

Equations for the three models are detailed below.

Slichter:

$$K = \frac{g}{v} 1 \times 10^{-2} n^{3.287} d_{10}^2 \quad (1)$$

Where,

g = acceleration due to gravity [LT^{-1}]

v = dynamic viscosity of water [$ML^{-1}T^{-1}$]

$n = \text{porosity } [-] = 0.255(1 + 0.83^{C_\mu})$

C_μ= the uniformity co-efficient given by the following formula:

$$C_\mu = \frac{d_{60}}{d_{10}}$$

d_{60}= grain size, where 60% of the sample is finer by weight

d_{10}= grain size, where 10% of the sample is finer by weight

Kozeny-Carmen:

$$K = \frac{g}{v} 8.3 \times 10^{-3} (\frac{n^3}{(1-n)^2}) d_{10}^2 \quad (2)$$

Beyer:

$$K = \frac{g}{v} 6 \times 10^{-4} (log \frac{500}{C_\mu}) d_{10}^2 \quad (3)$$

2.3 Bulk Density

There is a relationship between bulk density and porosity. Therefore, it is important to understand the physical sediment properties. The bulk density of the bulk (un-sieved) sediment samples were determined by placing the sediments in a 500 mL container of known weight and weighed. These were then dried in an oven at 60˚C and reweighed.

The bulk density of each sample was calculated using the equation:

$$\rho = \frac{m}{v} \quad (4)$$

Where, $\rho = \text{density } [\text{M}L^{-3}]$, m = mass [M], V = volume [L^3]

2.4 Porosity

Porosity was determined by filling a known volume with oven dried sediment and then slowly adding water until the sample was completely saturated. The weight of water added is the volume of the voids, as 1 g = 1 mL. Porosity, n [-], was calculated as the volume of the

voids divided by the total volume. Triplicates of each sample were measured, and an average taken.

2.5 RAD 7 Method for Measuring Radon

Radon equilibrium concentrations were measured on the different grain size fractions from the grain size analysis. Jars of individual grain sizes from the sieved sediments and bulk (un-sieved) samples, as shown in Figure 6a, were used to derive radon equilibrium concentrations.

The samples were sorted relating to the sample intervals in Table 1. There were 318 individual samples. Radon equilibrium concentrations for each sample were based on the measured radon activities from the saturated samples. These samples had been stored in sealed jars for 30 days to reach secular equilibrium (Chanyotha et al., 2014; Corbett et al., 1998; Sadat-Noori & Glamore, 2019). Radon activity was measured using the Durridge RAD7 (Durridge, 2020a), the Durridge RAD H_2O (Durridge, 2020b) and a Durridge active DRYSTIK in a closed loop system, as shown in Figures 6b and 6c. The RAD7 measures the radon activity by converting the alpha decay of the radon to an electrical signal (Durridge, 2020a). The radon concentration of the air entering the RAD7 allows the RAD7 to calculate the amount of radon in the water from the 40ml vial, using the WAT40 mode on the RAD7. The concentration of radon in the water sample is determined by the concentration of radon in the air loop (Durridge, 2020a).

2.5.1 Sample Preparation for Radon Emanation Experiments

Jars were filled with sediment samples and deionised water. They were placed in a cold store as temperature has been found to affect the rate at which radon diffuses from sediments (Durridge, 2020a; Sakoda et al., 2011); this would give misleading low equilibria.

Triplicates of each sample were made, as indicated by the sample intervals in Table 1, i.e., three 2mm samples from the same lithology and depth range. Due to the amount of sediment recovery, there were limited quantities of the smaller grain sizes. Therefore 125 mL jars were used for grain sizes 2 mm – <63 µm and 500 mL jars for the bulk sediments and grain size greater than 4mm.

In the current study, all samples initially were stored in glass jars with plastic lids. The plastic lids were made from high density polyethylene for the 125 mL jars and polypropylene for the 500 mL jars. Repeated emanation equilibria experiments were undertaken using glass jars with aluminium lids to ensure that there was no gas loss with the plastic lids. Plastic lids were replaced with aluminium lids with a parafilm seal, to see if this would increase our measurements of radon from the sediments. All of Selwyn 5 grain size fractions and bulk sediments were placed in jars with radon-free water. Bulk sediments from Selwyn 1, 3 and 7 were also used to give the spatial distribution of radon across the study site. The set-up shown in Figure 6. was used to analyse all the samples.

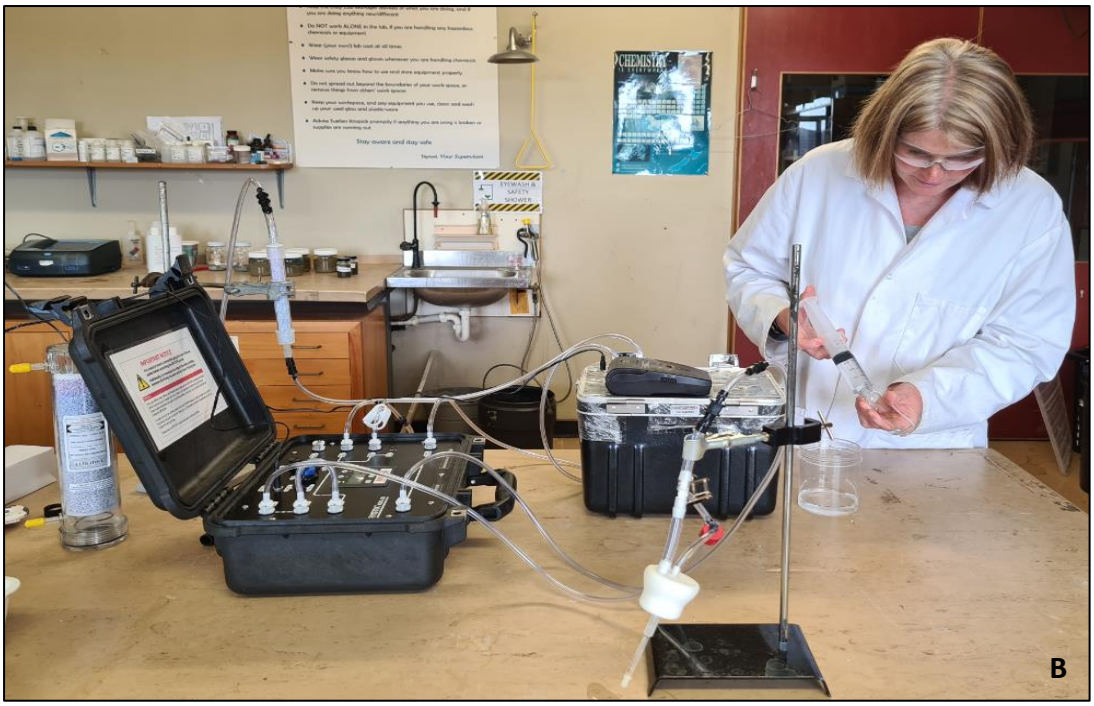

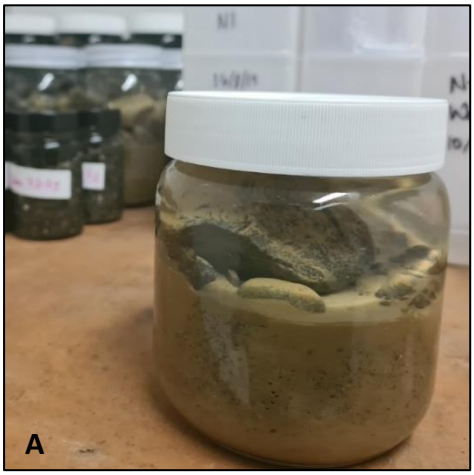

Sediments were stored for 30 days to reach secular equilibrium

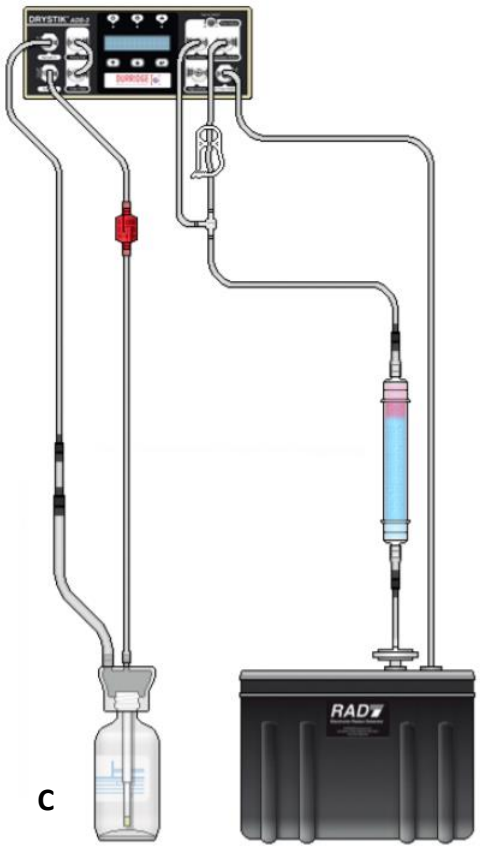

C -

Figure 6 A. Sediments in jars with DI water. loop setup. C. RAD 7, RAD H_20 and DRYSTIK

2.5.2 Experimental Setup for Measuring Radon

It was assumed that after 30 days of immersion the radon concentration in the water had reached equilibrium with the radon from the sediments. 40ml of water was then extracted

and analysed using the WAT40 method. The samples were aerated for 10 mins, to ensure all the radon was removed from the water. The equipment was purged for 5 minutes between samples to remove any radon from the tubes and the RAD7, as per the Rad7 manuals (Durridge, 2020a). A blank sample of degassed deionised water was measured between every 6-7 samples to ensure consistency in the measurements. The deionised water was degassed using a micrometrics ® AquaPrep™ II 056.

The initial experimentation was undertaken with tap water and deionised water from the laboratory. It was noted that the deionised water that was being used contained radon, however, the concentration was small, and therefore, after 30 days the initial concentration had decayed to an insignificant value.

When trialling the WAT40 set-up, humidity issues were identified which impacted on the measurement error. Different RAD7 units were tested to determine if the equipment was faulty, however, no difference was noted between the two units that were available. Further tests were conducted using two tubes of desiccant in series to determine if these were affecting the humidity results along with different settings for the pump. With the pump on 'Auto' the humidity stayed below 10%. If the humidity is above 10% it affects the sensitivity of the readings (Durridge, 2020a). The DRYSTIK mitigated the humidity issues as the airflow can be adjusted and also the pump alternated between on and off. The H_2O bypass was included in the set-up to control the air flow. The readings were low; therefore, a charcoal filter was introduced after purging to ensure all the radon was removed before the next sample was run, however, this made no difference. The WAT 40 method is programmed for 4 cycles, with a cycle time of 5 minutes, however, this gave high uncertainties. To reduce the uncertainty the counting time was increased to 10 five - minute

cycles. Therefore, every sample took one hour to process. The DRYSTIK reduced the amount of desiccant required and kept the humidity (RH) below 10%. The DRYSTIK has a high air flow and low air flow option. The high air flow was found to increase the chances of foaming. Different aeration times with the high and low air flow were investigated. Following from this we used the low air flow with an aeration time of 10 minutes. When using the low air flow, it is recommended to have a cycle time of 10 minutes, therefore we changed to a cycle time of 10 minutes, with a recycle of 5 minutes. To ensure no air was introduced into the sample the syringe and tube were filled with DI water and any air pushed out before sampling from the jars.

After completion of the emanation rates for sediment samples from borehole Selwyn 5, a groundwater sample was taken and analysed using the WAT40 method. The groundwater sample was considerably higher in radon than the sediments. It was thought that perhaps there was gas diffusing through the plastic lid. To determine if this was the case additional experiments were undertaken to test if the samples were reaching equilibrium.

2.5.3 Radon Emanation Rate Sample Method Testing

To test if the sediments were reaching radon equilibrium concentrations, six 500 mL jars, three with plastic polypropylene lids, and three with aluminium lids and parafilm were used, and the water analysed. A comparison of the 125 mL jars with the high-density polyethylene and metal lids was also undertaken. Using sediments from the same depth and lithology the samples were allowed to sit for 5 days, then 40 mL of water extracted and analysed. The sediments were dried and put back into jars with radon free water and allowed to sit for 10 days and the water analysed. The process was then repeated for 15 days and 20 days. To

ensure the radon in the water is in equilibrium with the radon produced by the sediments the samples need to sit for >20 days (Chanyotha et al., 2016).

2.5.4 Testing Bentonite as a Potential Source of Radon in Constructed Piezometers and Granite as a Known Radioactive Source

It was thought that with the vertical movement of the water, some of the water may have contacted the bentonite clay along its flow path. The bentonite clay was used to seal the annulus of the well and to prevent preferential flow along the well casing. The contact between the bentonite and the water could have elevated radon concentrations in the groundwater samples. Therefore, three 500 mL jars were filled with bentonite and radon free water with an aluminium lid and parafilm seal and placed in a cold store for 30 days to reach equilibrium and analysed as per the previous emanation equilibria experiments.

Granite is known to contain radioactive material. Therefore, as a comparison with the sediments from the Waikirikiri Selwyn River three jars with aluminium lids were filled with granite (Karamea Batholith) and radon-free water and allowed to sit for 30 days in a cold store. These granite samples were analysed as per the previous emanation equilibria experiments.

2.6 Data Analysis

The Durridge Capture® software is a tool that communicates between the RAD7 and the Windows operating system and allows for analysis of the radon data. Each individual analysis, a run, has a corresponding printout as shown in Figure 7. The radon concentration in the water is measured with the associated uncertainty for every cycle and an average given for each run, along with the temperature and humidity. Column A (Polonium 214) and column C (Polonium 218) are emitted when radon decays (Durridge, 2020a). The

uncertainty with the radon in water concentrations is calculated by the RAD7 using 1 + SQR(N+1), where N is the number of counts (Durridge, 2020a).

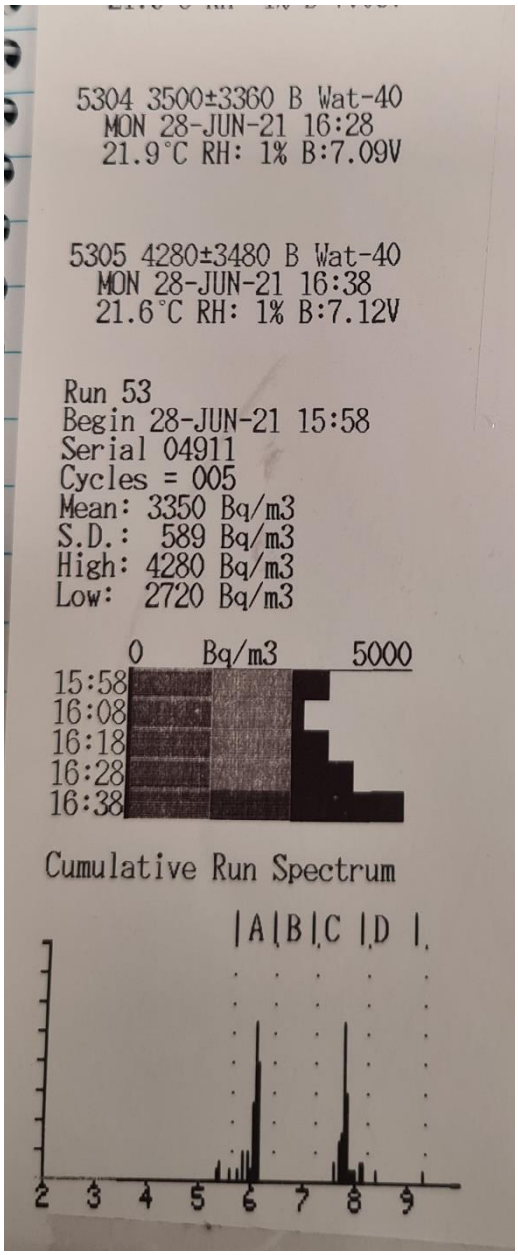

Figure 7 RAD H_20 printout from a radon equilibrium concentration analysis.

The Capture software displays the data as shown in Figure 8a. The average concentration of radon in water for the triplicate samples was calculated using the Durridge Capture® software, an example of which is shown in Figure 8b.

A

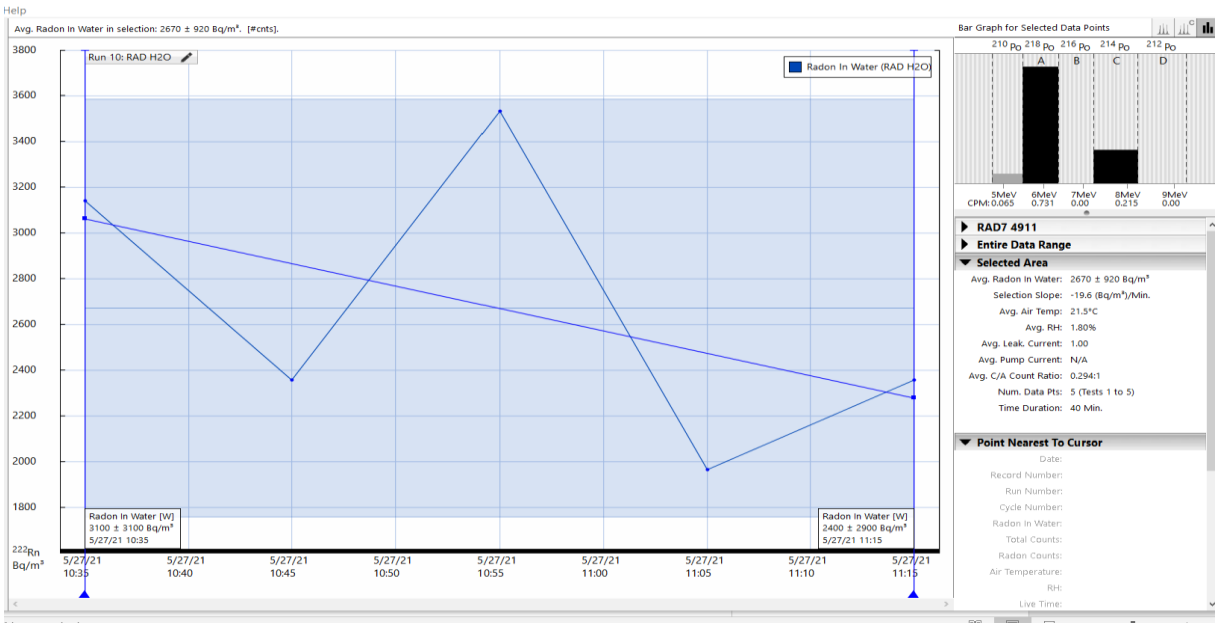

B

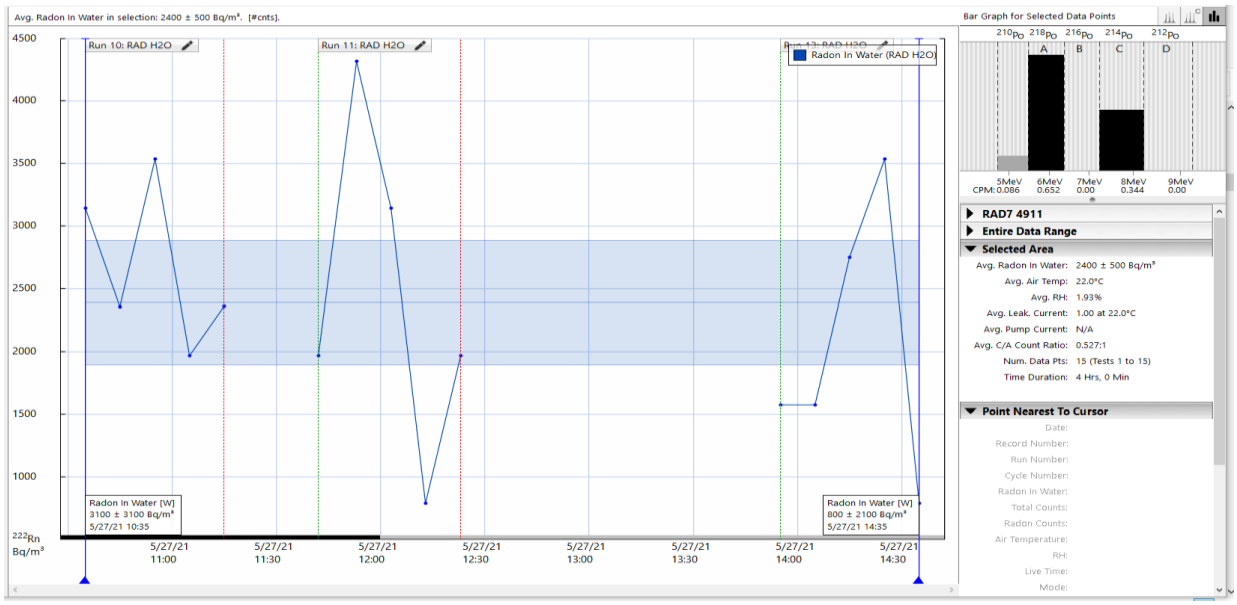

Figure 8 A Example of the measured data in the Durridge Capture software. B Radon data for three runs combined together.

The radon emanation equilibria concentration, from the collected sediment samples, was calculated using equation (5) as per Mullinger et al. (2009).

$$E_{Rn} = \frac{Rn \times V_w}{M} \quad (5)$$

Where E_{Rn} = radon emanating from the sediment sample (Bq/kg)

Rn = radon equilibrium concentration in the water (Bq/L)

V_w = volume of water in the jar (L)

M = mass of the sediment in the jar (kg).

2.7 Groundwater Sampling for Radon-222

Groundwater samples were taken from piezometers 5, 1 and 7. These were analysed using the WAT40 method to give a direct comparison of the groundwater radon concentration and the radon equilibria concentrations from the bulk samples. Piezometers were purged, using a submersible pump, to ensure a representative sample was collected. Water levels were recorded in the piezometers before purging to remove three standing piezometer volumes (Close et al., 2014). Field measurements at these locations were taken of electrical conductivity, pH, DO and temperature using a Solinst datalogger. To ensure the water had not been in contact with air, the water was pumped into a deep container and allowed to overflow, with the tube being placed at the bottom of the container. Three 40 mL vials were filled up from the bottom of the container and sealed under water.

2.8 Liquid Scintillation Counting Method

Liquid Scintillation counting is an established method for counting radon (Schubert et al., 2014). Three water samples from bulk sediments from the sample 6.0–7.5 m and three

water samples from the <63 µm sediments were sampled. This was the same sediment that was used for the radon emanation rate experiments. Each vial was filled with 10 mL scintillant (Opti-Fluor O). 10 mL of sample water was slowly extracted from the jars to minimise degassing. The syringe needle was then placed at the bottom of the vial to ensure the sample water was placed in the vial underneath the scintillation cocktail to minimise degassing of the water. The vial was then sealed and shaken. The samples were sent to GNS Laboratories in Wellington for analysis.

3 Results

3.1 Particle Size Distribution

Analysis of the particle size distribution curves revealed that the majority of samples contained sediments ranging in size from 31.5 mm down to 0.004 mm, i.e., from pebbles to clays. Figures 9 to 13 show the particle size distribution curves of the sieved sediments based on the sample intervals from Table 1 for the five drillholes (Selwyn 1, 3, 5, 7 and 9).

Figure 9 shows the particle size distribution curves, for each sample interval for Selwyn 1. As can be seen, the differing percentages of sediments result in varying curves. These curves generally follow a similar pattern, except the sampling interval 10.52–11.1 m, which contains a greater amount of sand.

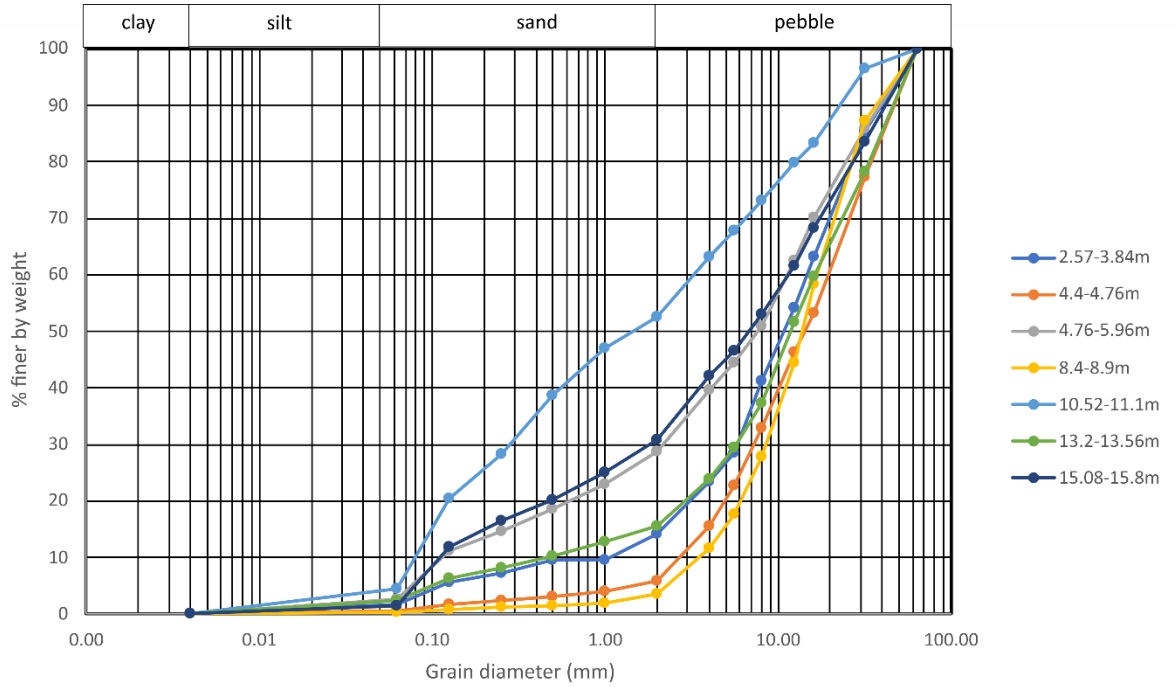

Figure 9 Particle size distribution curve for sample intervals in Selwyn 1.

Selwyn 3 (Figure 10) shows no similarities between curves. Sample interval 13.56– 14.4 m has a larger volume of coarse sand and pebbles, in comparison to the other sample intervals

for Selwyn 3. The other sample intervals have more finer sand. The percentage recovery for 13.56-14.4 m was 60%.

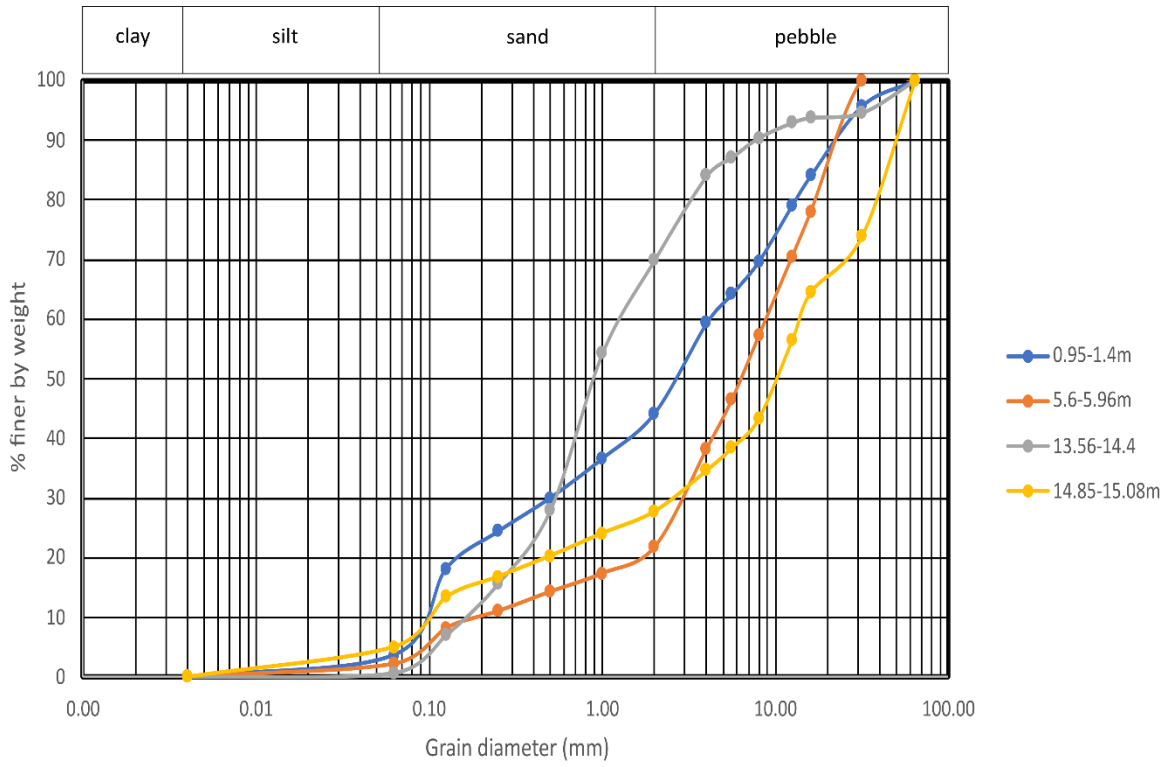

Figure 10 Particle size distribution curves for sample intervals for Selwyn 3.

The sample depths in Selwyn 5 (Figure 11) display a greater amount of similarity than the distribution curves of Selwyn 1 and 3. Sample interval 7.8–10.5 m, shows a slightly greater volume of coarse sand than the other sample intervals. Sample interval 14–15 m shows the greatest amount of sand and silt, but only 60% of the sediment was recovered for this interval. In comparison to Selwyn 1, the lithology of Selwyn 5 overall contains more sand, however there was a greater volume of recovery from Selwyn 5 than Selwyn 1.

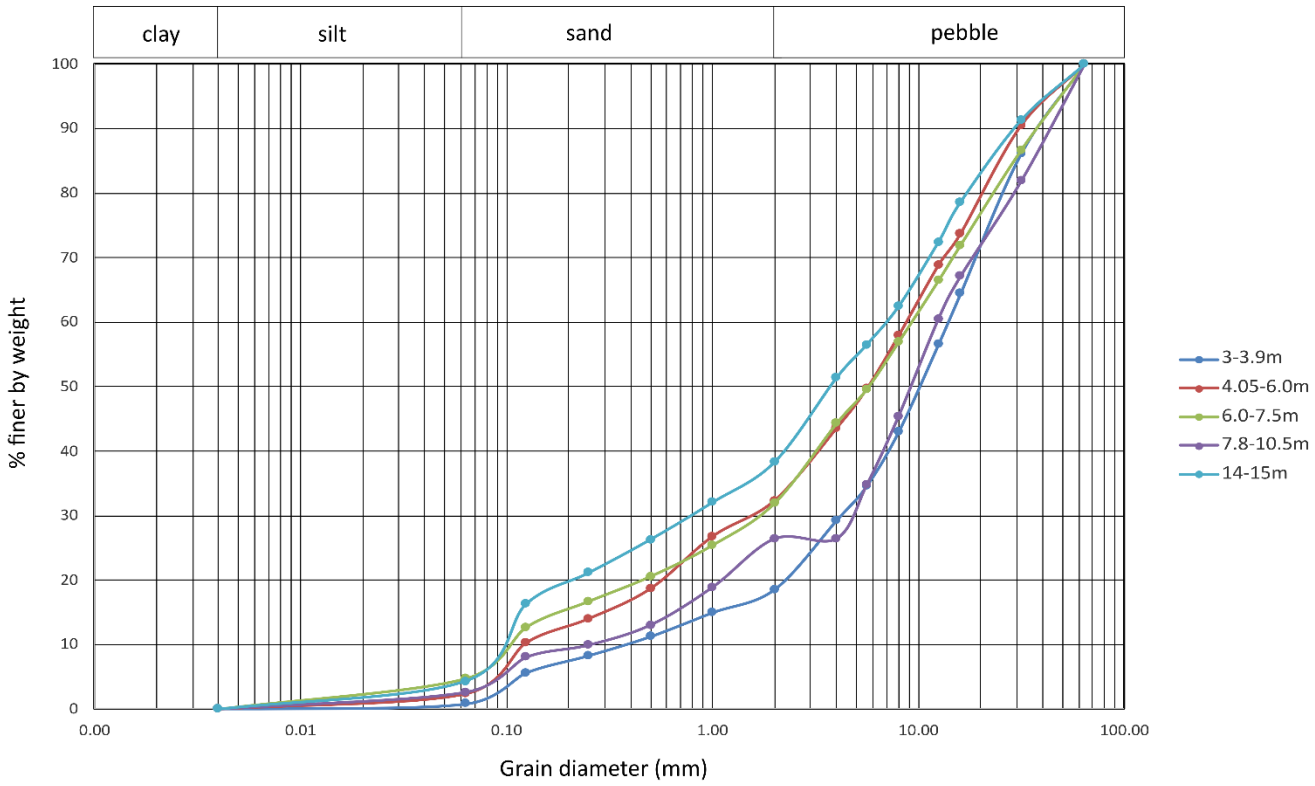

Figure 11 Particle size distribution curve for sampling intervals in Selwyn 5.

Selwyn 7 only has one sampling interval, however, this follows a similar distribution curve to the curves of Selwyn 5.

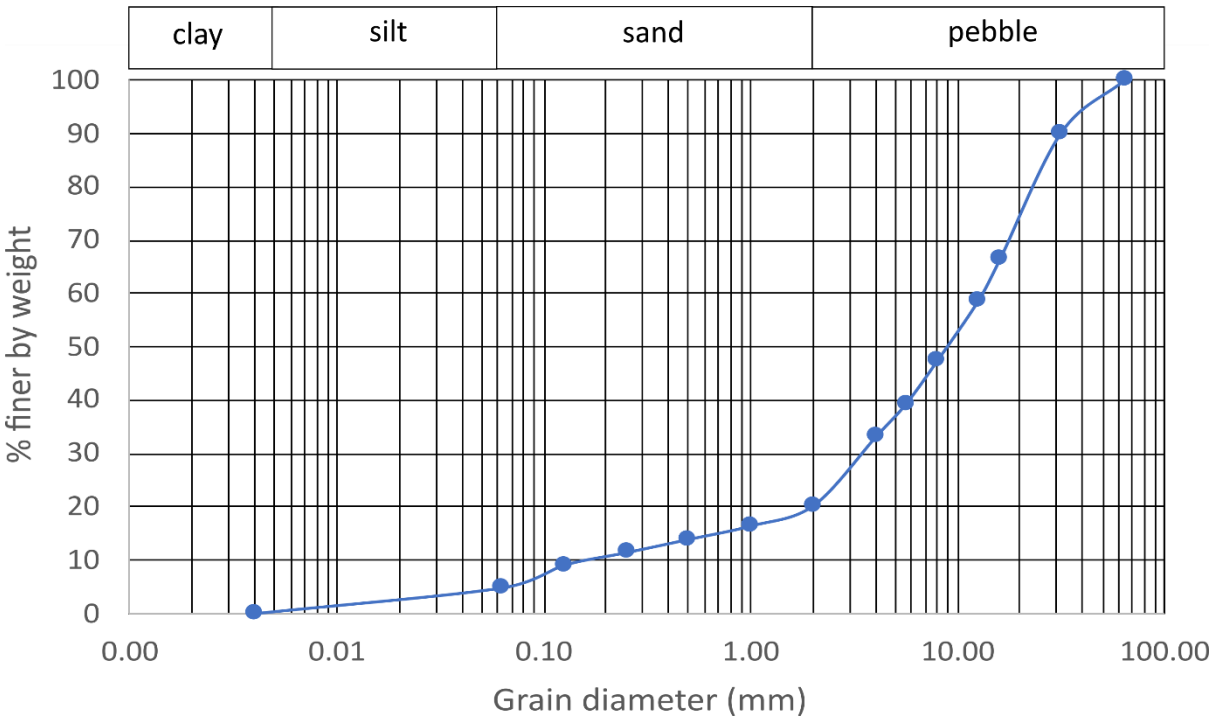

Figure 12 Particle size distribution curve for Selwyn 7.

The limited recovery of sediments from Selwyn 9 is evident in the lack of sands and silts in comparison to other wells. The majority of the recovered sediment from Selwyn 9 was pebbles (Figure 13).

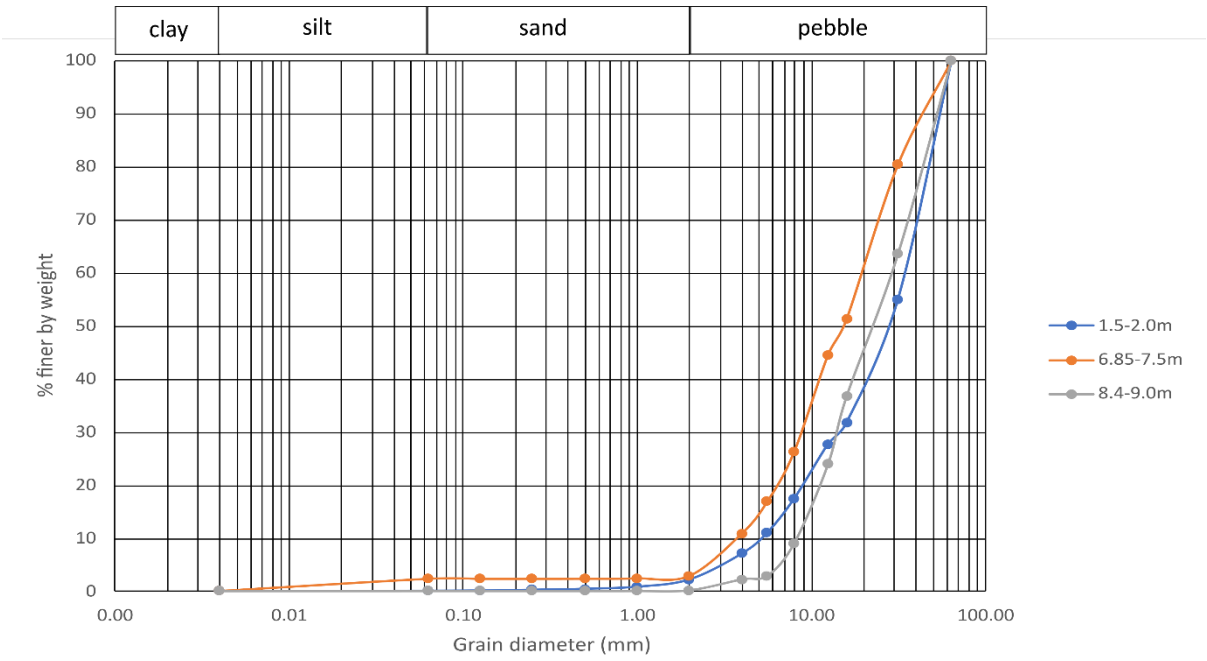

Figure 13 Particle size distribution curve for sampling intervals of Selwyn 9.

3.2 Hydraulic Conductivity, Bulk Density and Porosity

From the particle size distribution curves shown in Figures 9 to 13, in which the grain size at which 60% and 10% finer were extracted, the uniformity coefficient for each distribution curve was calculated as well as the hydraulic conductivity using the three different models as described in Section 2.4. Figure 14 shows the results of the three different models for the sample intervals. Appendix A shows the hydraulic conductivities calculated.

Selwyn 9 and Selwyn 1, depth 8.4-8.9m, where there was limited recovery, have increased conductivities. The results from Selwyn 9 have not been presented due to the calculated hydraulic conductivity values being unrealistically high.

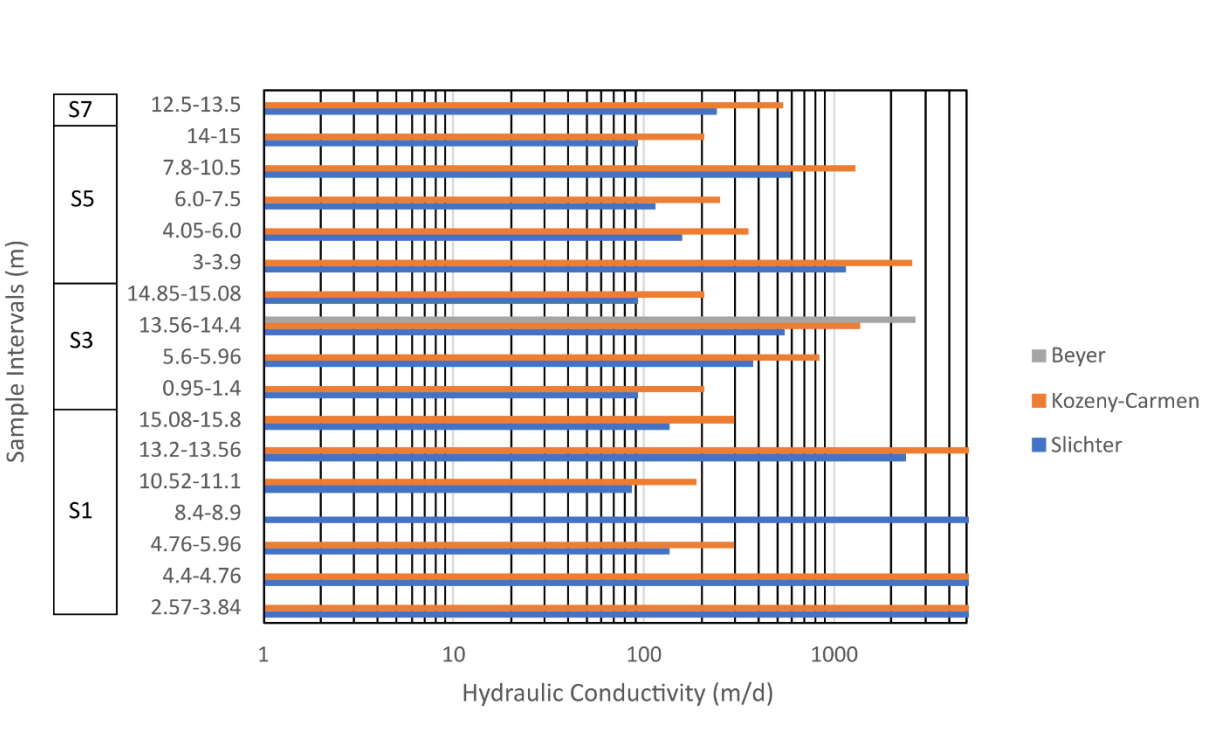

Figure 14 Hydraulic conductivities calculated via three different models.

However, conditions need to be met for formulas to apply. When using the Slichter equation d_{10} should be between 0.01-5 mm. The Kozeny-Carman is generally applied to silts and sands and d_{10} <3 mm. The Beyer formula should have C_u between 1 and 20 and d_{10} between 0.06 - 0.6 mm. When you apply these conditions to the results in the table, the Slichter and Kozeny-Carman conditions are nearly always met as they only depend on the value of d_{10}. The conditions for the Beyer formula are only met for sample interval 13.56–14.4 from Selwyn 3.

Bore logs have been drawn for each of the wells sampled, showing calculated hydraulic conductivity, measured bulk density and porosity. Porosity was only measured for all the sampled depths of Selwyn 5 and the deepest sampling intervals of Selwyn 1, 3 and 7, due to time constraints.

Figure 15 shows the bore log for Selwyn 1. The porosity was only measured for the sampling interval 15.08-15.8m of Selwyn 1 and this was 0.22. This is similar to the values obtained for Selwyn 5 which ranged from 0.18-0.25. The hydraulic conductivity estimates vary throughout the well, and generally show higher values for samples with low sediment recovery, where the silts and clays have been washed away during the drilling process. The conductivity calculated for sample interval 15.08-15.8 m ranges between 140-700 m / d. This is a more realistic value in comparison to the conductivity calculated from sample interval 2.57–3.84 m which has a starting range of 11,000 m / d.

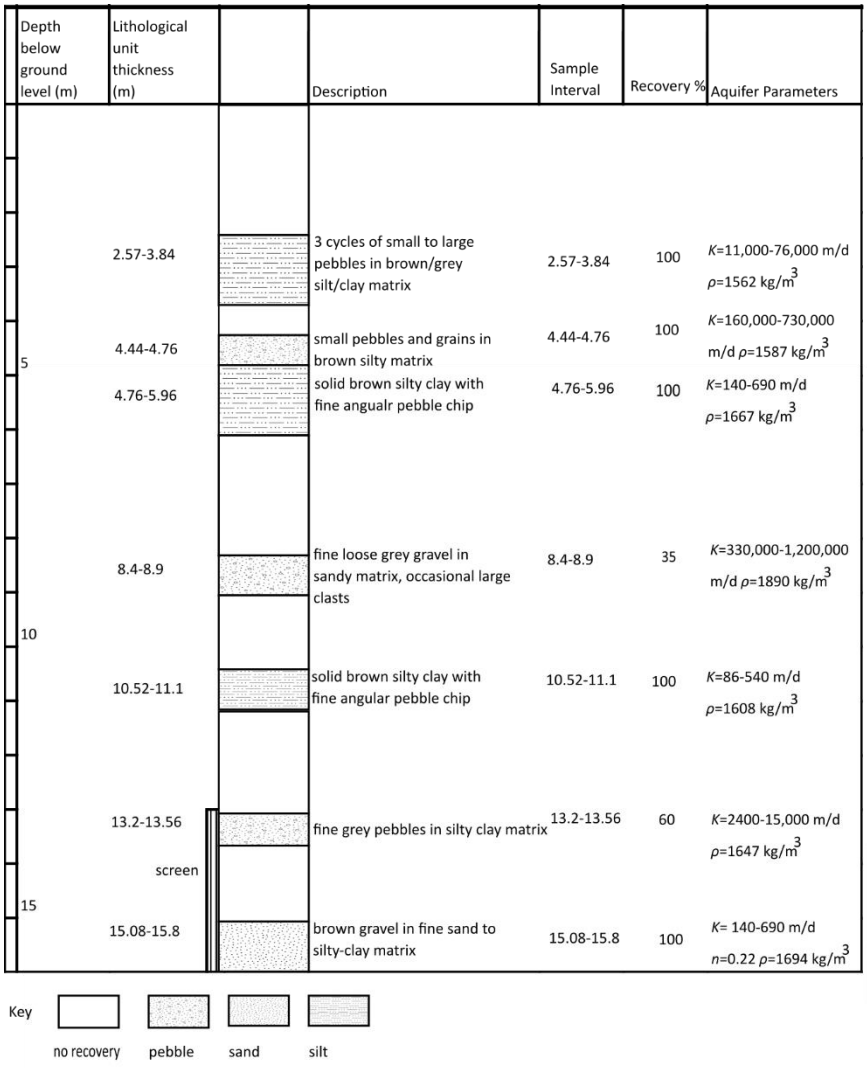

Figure 15 Bore log of Selwyn 1, including measured and calculated hydraulic conductivity, porosity and bulk density values.

The porosity measured for sample interval 14.85–15.08 m from Selwyn 3 is 0.3. This is slightly higher than the values measured for Selwyn 5 which had a range of 0.18–0.25 and Selwyn 1 which was 0.22. However, due to the small amount of sediment available to estimate porosity, small jars had to be used, which are difficult to pack. Thus, this porosity value serves as a guide as opposed to a more realistic value. The conductivity for Selwyn 3 ranges from 94 m / d at a depth of 14.85–15.08 m to 2700 m / d for sample interval 13.56– 14.4 m. From the particle size distribution curves, Selwyn 3 has larger amounts of

sand overall compared with the other wells, leading to lower hydraulic conductivity ranges for the sample intervals. The bulk density ranges from 1450 kg/m^3 to 1750 kg/m^3.

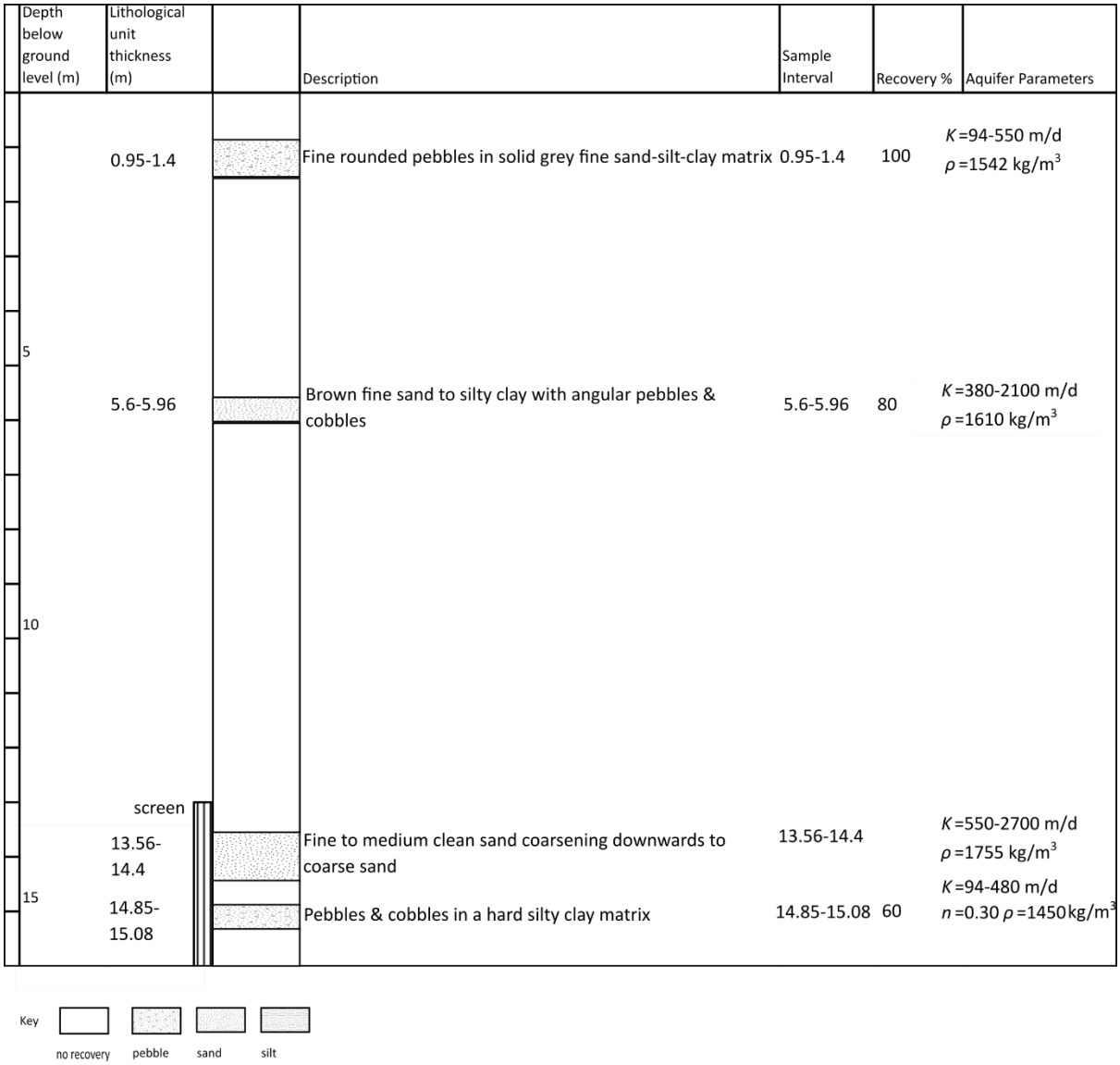

Figure 16 Bore log of Selwyn 3, including measured and calculated hydraulic conductivity, porosity and bulk density values.

Figure 17 shows the variation of conductivity, porosity and density values within well 5. Porosity varies throughout the depth of the well, but within a range of 0.18–0.25. Hydraulic conductivity ranges from 94 to 80 m / d at 14–15 m depth, correlating to the larger volumes of silts and clays, followed by the sample interval 6.0–7.5 m, which had the second largest

volume of silts and clays. From sample interval 3–3.9 m this has the largest conductivity range, however, there was only 60% recovery from 3–3.5 m, suggesting that the fines may have been washed away when drilling this section.

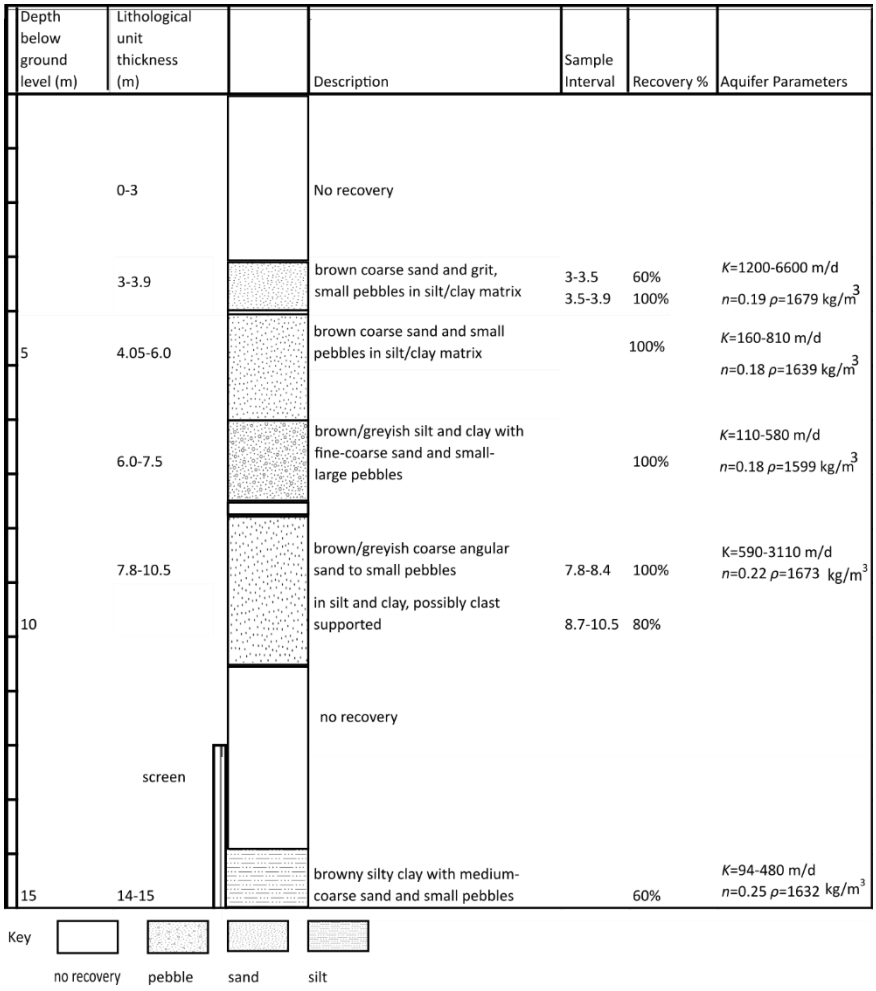

Figure 17 Bore log of Selwyn 5, including measured and calculated hydraulic conductivity, porosity and bulk density.

Figure 18 shows the results for Selwyn 7. As can be seen, there was very limited recovery for this well. The measured porosity and hydraulic conductivity values for Selwyn 7 were within the range obtained for Selwyn 5.

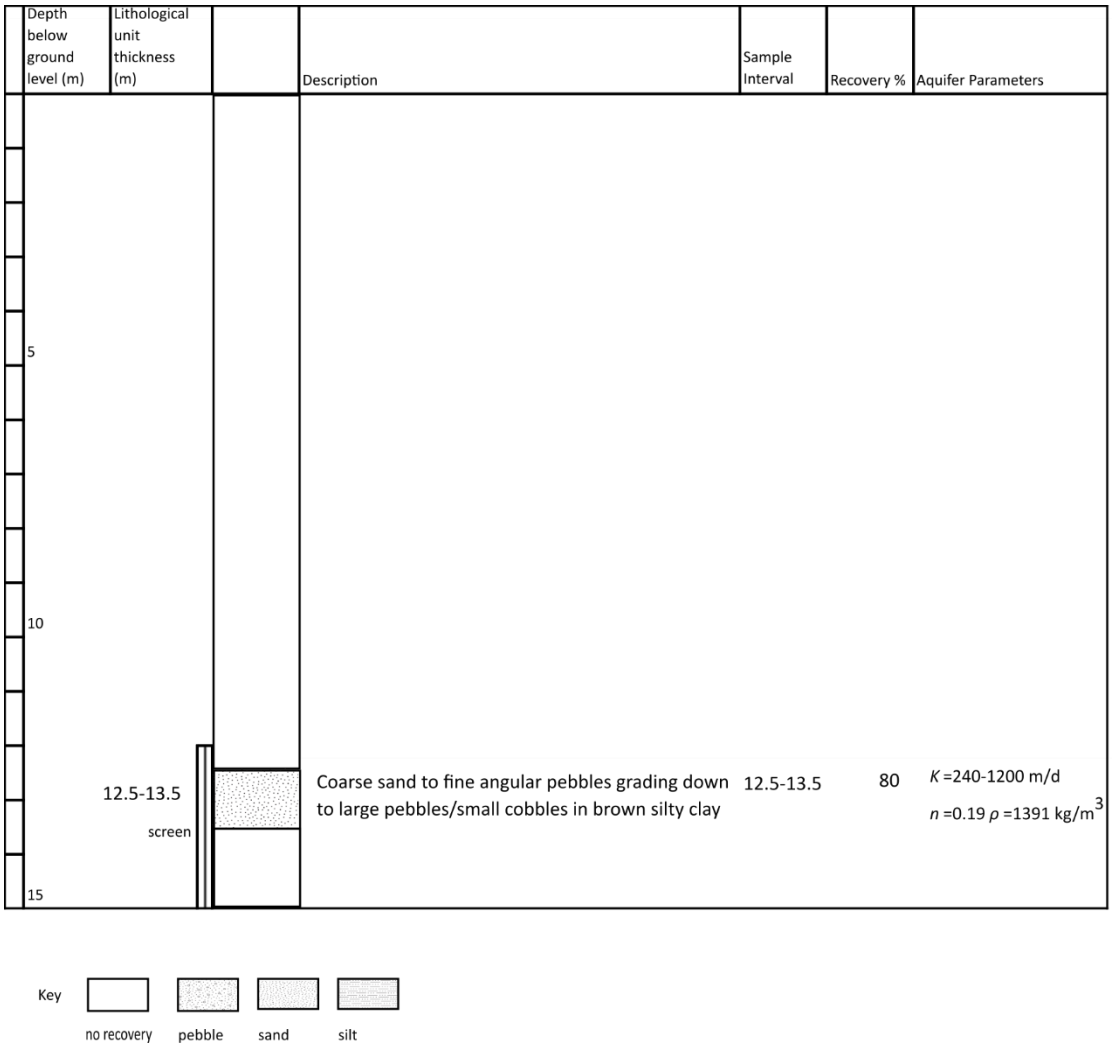

Figure 18 Bore log of Selwyn 7, including measured and calculated hydraulic conductivity, porosity and bulk density values.

In Selwyn 9 (Figure 19), the limited sediment recovery from drilling has influenced the calculated hydraulic conductivity values, potentially biasing results with the higher proportion of larger grain sizes. Porosity was not measured on sediment samples collected from this drillhole due to the limited recovery of sediment during drilling.

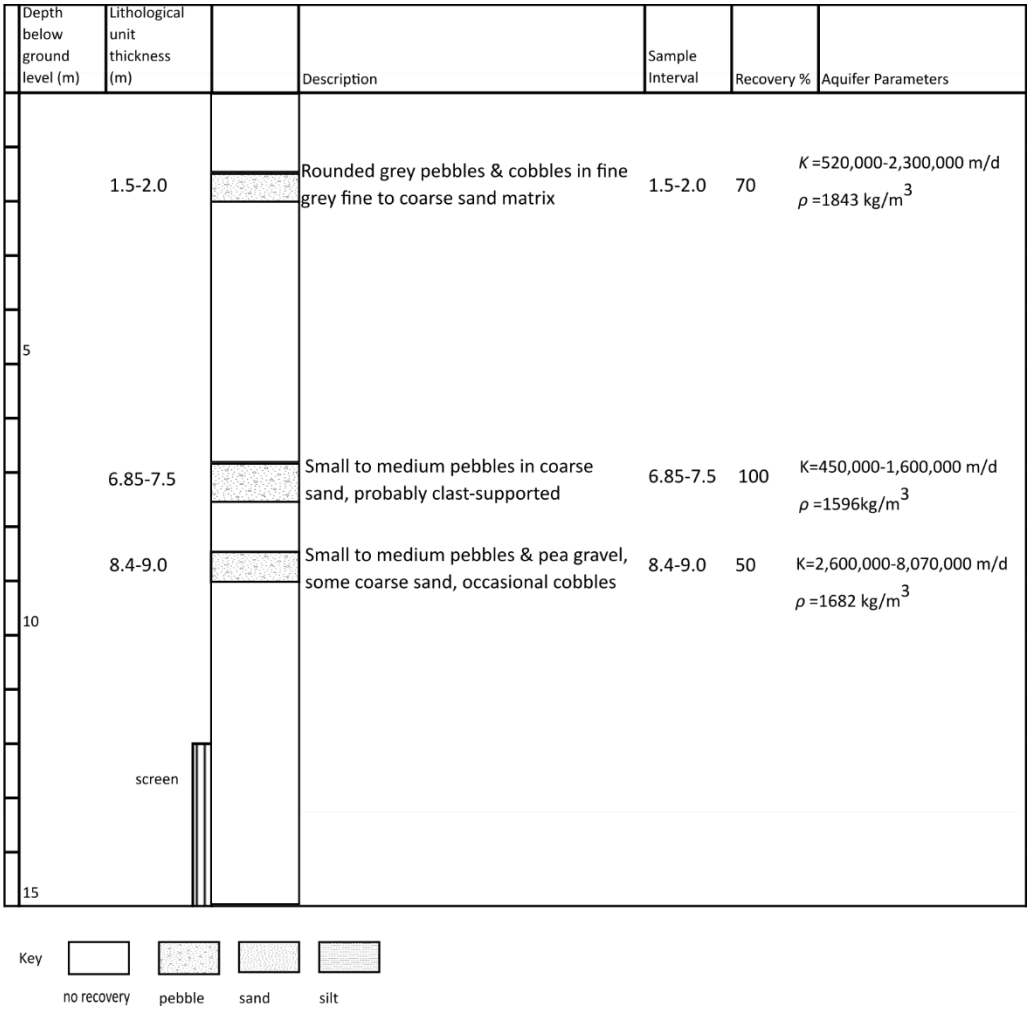

Figure 19 Bore log of Selwyn 9, including measured and calculated hydraulic conductivity, porosity and bulk density values.

3.3 Radon Equilibrium Concentrations

3.3.1 Comparison of Radon Equilibrium Concentrations Across Grain Sizes

Radon concentrations in water were compared for different grain sizes within the same sample interval using jars with metal lids. Figure 20, shows how the grain size varies with each sample interval of Selwyn 5. It is evident for all sample intervals that the <0.0063 mm sediments produce a greater amount of radon than the other grain sizes. For example, in sample interval 6.0–7.5 m, the <0.0063 mm fraction has a radon concentration of 3.77 Bq/L, in comparison to the > 0.5 mm fraction which has a radon concentration of 0.6 Bq/L. Figure

20 shows that the bulk samples from all sample intervals have higher radon concentrations than the individual grain size fractions, the only exception being the <0.0063 mm fraction. The error bars on the radon in water concentrations in Figure 20 are calculated as per section 2.6.

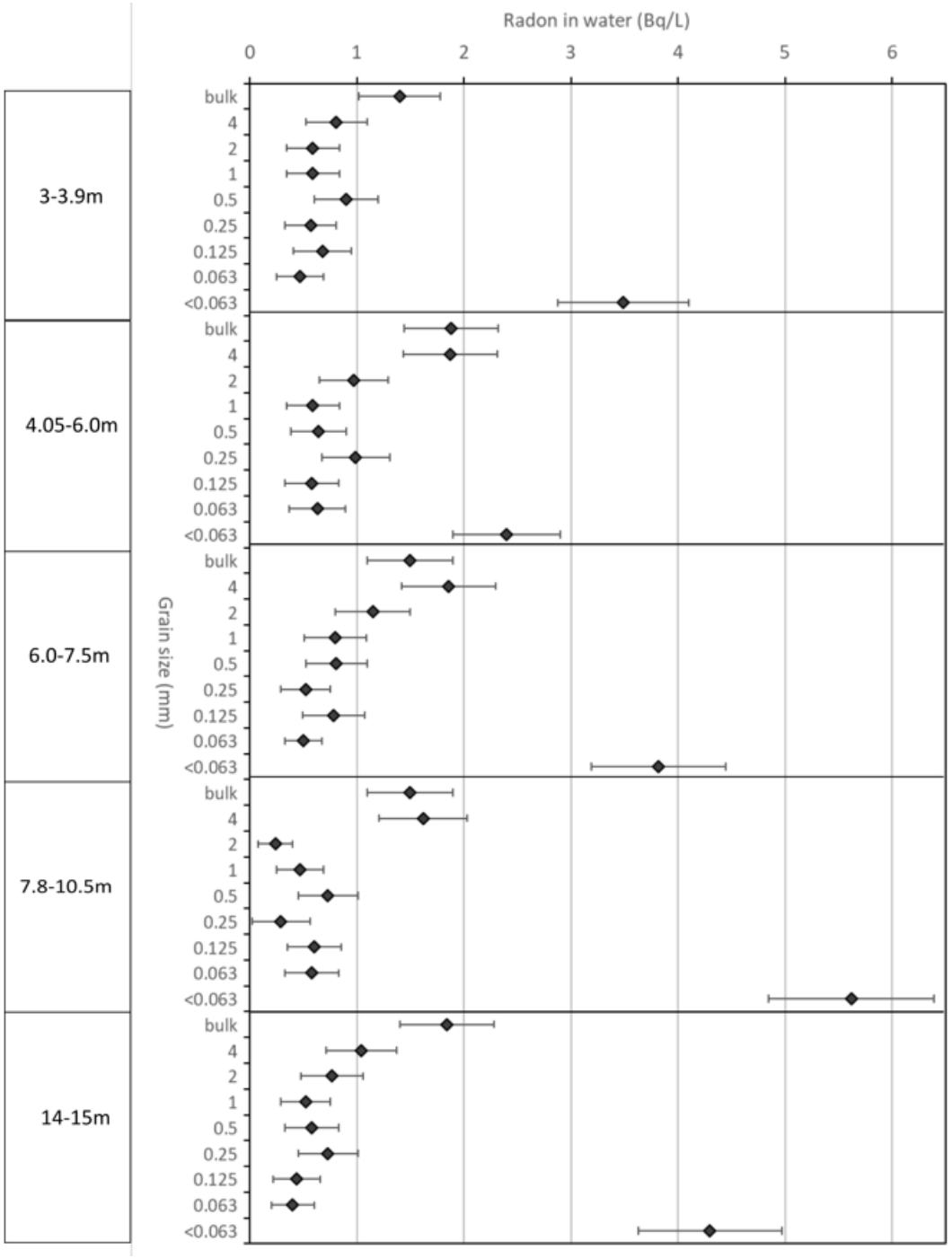

Figure 20 Radon equilibrium concentrations for different grain sizes in the sample intervals for Selwyn 5 for jars with metal lids.

3.3.2 Comparison of Grain Size with Depth

The radon equilibrium concentration for each grain size fraction was compared among all the sampling intervals of Selwyn 5.

Figures 21 and 22 show the variation of radon concentration in the extracted water with sampled depth for the >2mm and the <0.63 µm grain sizes respectively in Selwyn 5. The >2mm sediments range from 0.49–1.04 Bq/L, and the <0.63 µm range from 3.56–4.6 Bq/L. There is no significant variation with depth when the error bars are taken into consideration. Appendix D shows the results for all the grain sizes.

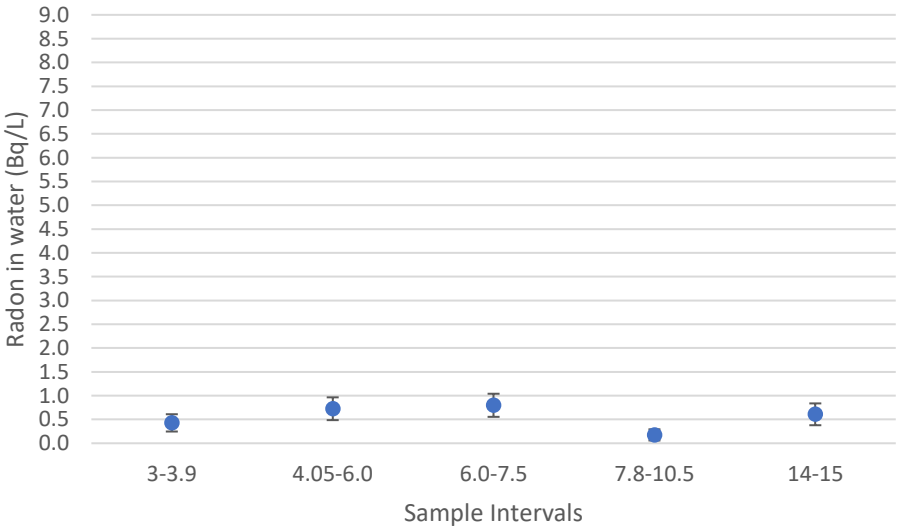

Figure 21 Variation of radon concentration with sample depth for the >2mm grain size for jars with metal lids in Selwyn 5.

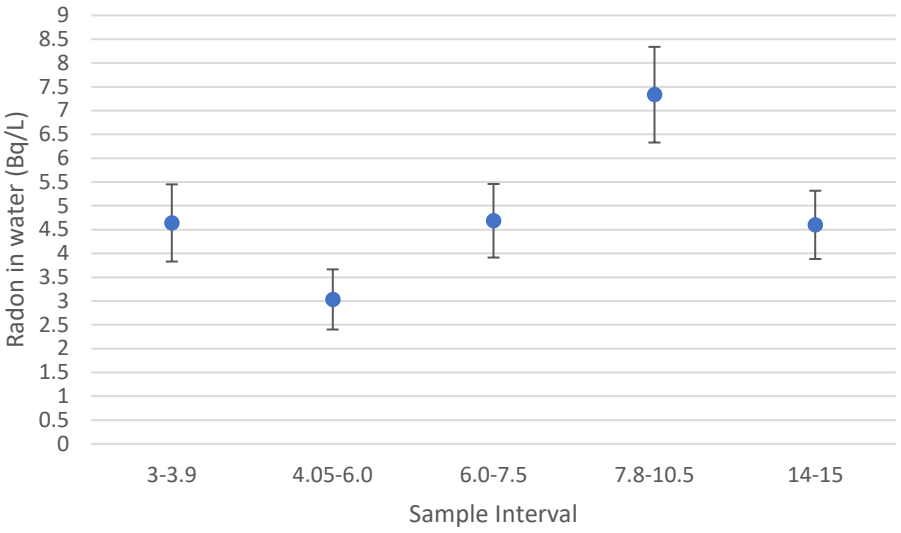

Figure 22 Variation of radon concentration with sample depth for the <63micron grain size for jars with metal lids in Selwyn 5.

3.3.3 Radon Equilibrium Concentrations Across the Study Site

Figure 23 shows the variation of radon equilibrium concentration from the sediments across the study site according to sample interval, using jars with metal lids. The range of radon concentration values is 0.6–1.88 Bq/L. The two smallest values are from Selwyn 1, 8.4–8.9 m, 0.6 Bq/L and Selwyn 3, 13.56–14.4 m, 0.63 Bq/L. Both of these samples had a larger amount of coarser material compared to the other samples with metal lids.

If we compare the radon concentrations to their associated source lithology, it appears that the radon concentrations increase with depth in each of the formations. For example, in Selwyn 1, 3 and 5 the sample results show an increase in radon concentration with depth to 6m, where the Springston Formation ends. Samples below this depth are from the Burnham Formation, and show a pattern of increasing radon concentration with depth. Within the postglacial sediments of the Springston Formation, radon is low near the surface, and is higher towards the contact with the Burnham Formation at around 6 m. The radon

concentration is low at the top of the Burnham Formation and increases as the sample intervals go deeper.

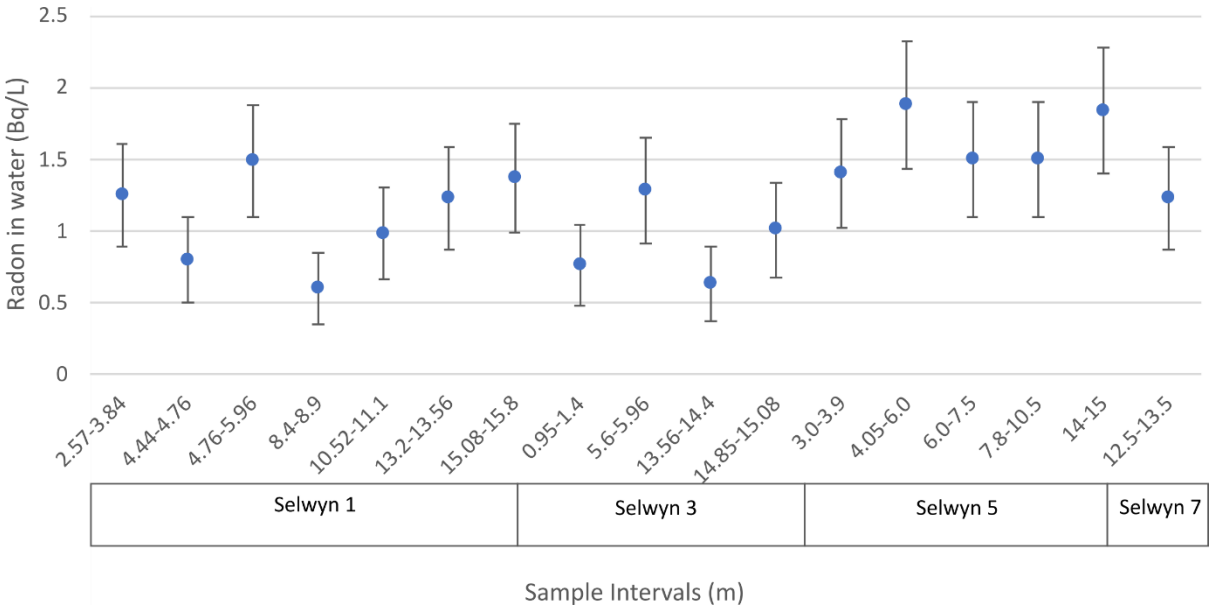

Figure 23 Spatial distribution of radon emanation across the study site according to sample depth for jars with metal lids.

A comparison between radon equilibrium concentrations from water held in glass jars with plastic lids and metal lids was undertaken to ensure there was no gas loss from the plastic lids. The results in Figure 24 show that there was little difference in radon concentration between the two sets of experiments.

A

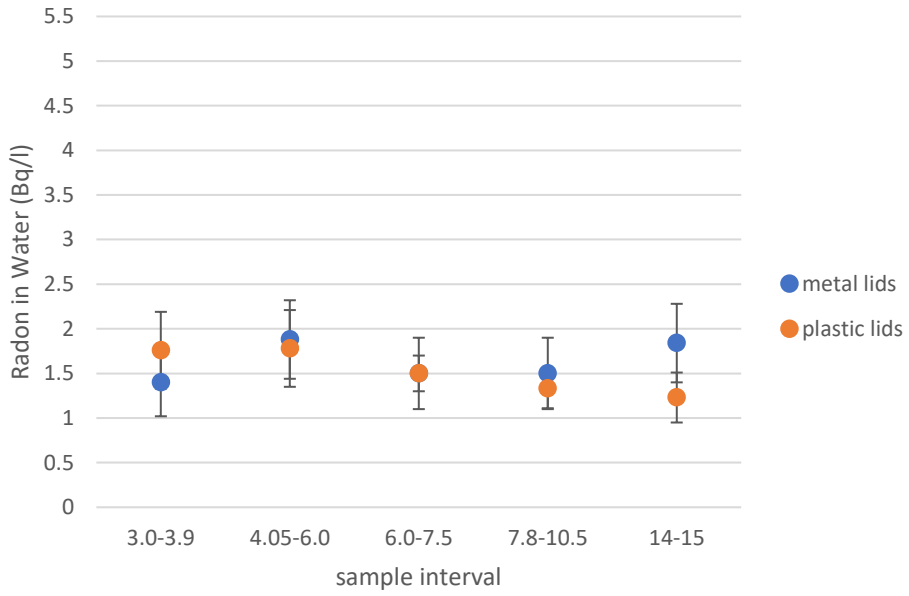

B

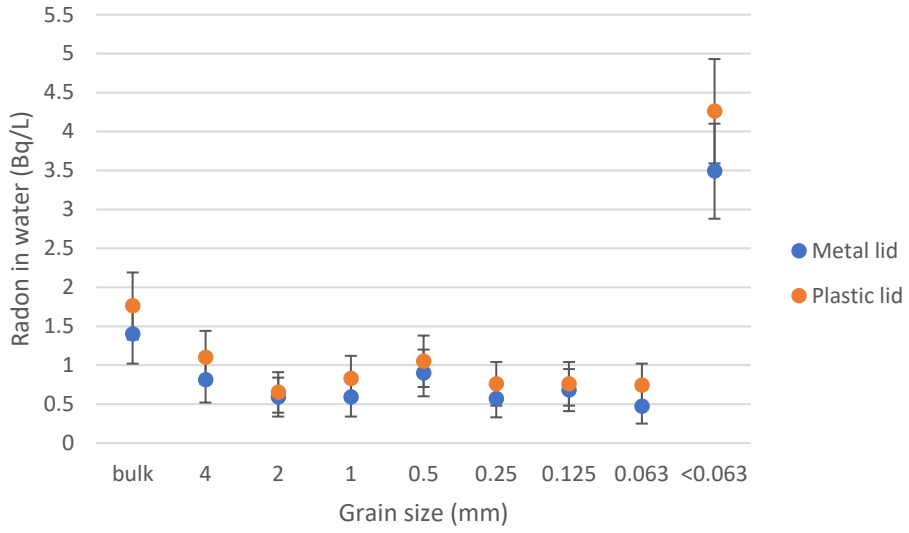

Figure 24 Comparison of radon concentrations for samples stored in jars with metal and plastic lids for bulk samples in Selwyn 5 (A) and for different grain size fractions from sample interval 3-3.9 m in Selwyn 5 (B).

3.3.4 Radon Emanation Rate Test Comparison

Analysis was undertaken of the radon concentrations of the water from the 500 mL jars with plastic lids and 500 mL jars with metal lids, both filled with bulk samples from the same

sample interval, 6.0–7.5 m, from Selwyn 5. The experiment was also undertaken using 125 mL jars with plastic and metal lids using the <63 µm fraction of the 6.0–7.5 m sample interval. The analysis of the radon emanation rates from these samples are shown in Figures 25 and 26. From the results it appears that the water from the jars may not be reaching equilibrium as the results from 10-20 days of immersion are very similar to each other.

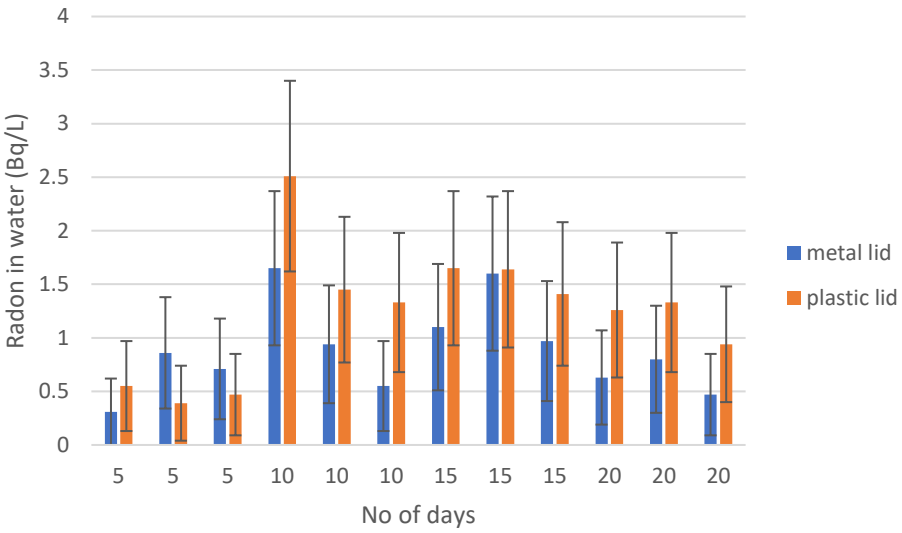

Figure 25 Radon emanation rate analysis of the water sampled from 500 mL jars containing bulk sediments.

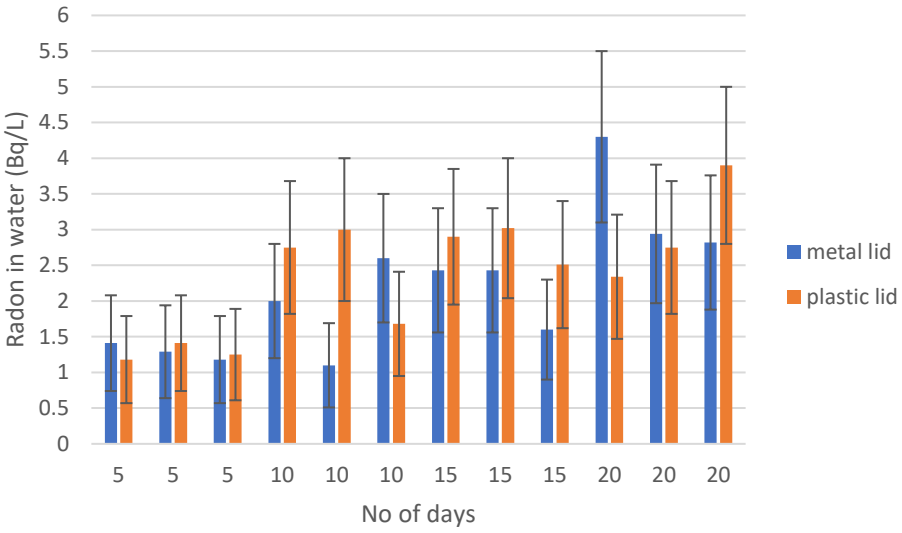

Figure 26 Radon emanation rate analysis of the water sampled from 125ml jars containing sediment of 63µm.

3.3.5 Radon Liquid Scintillation Counting

The radon equilibrium concentration from the liquid scintillation counting for the bulk samples from sample interval 6.0–7.5 m, from Selwyn 5, ranges from 2.18 to 4 Bq/L ± 0.17 Bq/L. In comparison, the radon concentrations measured for the same sample interval using the RAD7 ranged from 1.1 ± 0.59 Bq/L to 1.8 ± 0.74 Bq/L. The comparison of the radon concentration using the two analysis methods is shown in Figure 27.

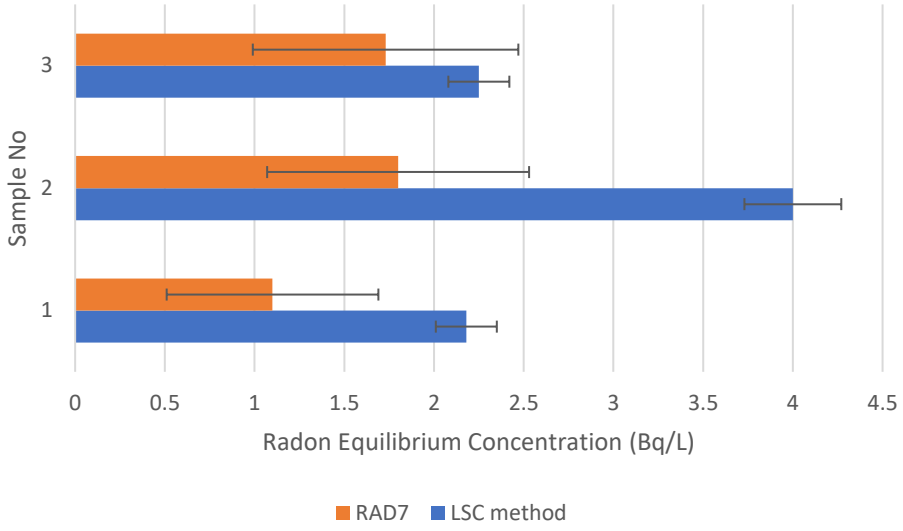

Figure 27 Comparison of radon equilibrium water concentrations using RAD7 and LSC method for bulk samples.

Figure 28 shows the comparison of radon equilibrium concentration determined by the two analysis methods for the <63 µm sediment fractions from the same sample interval (6.0– 7.5 m). The radon concentration using the liquid scintillation counting (LSC) method ranged from 3.65 ± 0.25 Bq/L to 5.01 ± 0.33 Bq/L. The radon concentration from the RAD7 for the same sediments ranged from 3.0 ± 1.0 Bq/L to 4.6 ± 1.2 Bq/L.

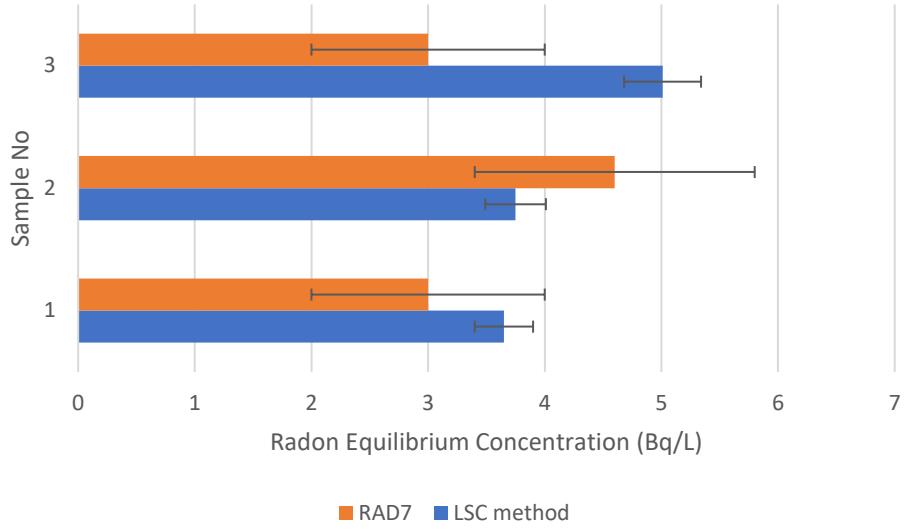

Figure 28 Comparison of radon equilibrium water concentrations for <63µm using RAD7 and LSC method

3.4 Analysis of Bentonite and Granite

The radon equilibrium concentration from the bentonite clay ranged from 0.47 ± 0.38 Bq/L to 1.05 ± 0.58 Bq/L.

The radon concentration of a known radioactive source was analysed to compare with the radon equilibrium concentration from the sediments from beneath the Waikirikiri Selwyn River. The radon concentration from the ground granite ranged from 0.63 ± 0.44 Bq/L to 1.73 ± 0.74 Bq/L.

3.5 Groundwater Sampling

The radon concentration in the water for Selwyn 1 ranges from 2.48 ± 0.92 Bq/L to 2.76 ± 0.99 Bq/L (Figure 29). Selwyn 5 ranges from 16.48 ± 2.29 Bq/L to 19.05 ± 2.55 Bq/L. Selwyn 7 ranges from 5.31 ± 1.30 Bq/L to 6.5 ± 1.44 Bq/L. When compared to the radon in water samples from the sediments from these piezometers these ranged from 0.58 d± 0.44 Bq/L to 2.65 ± 0.91 Bq/L.

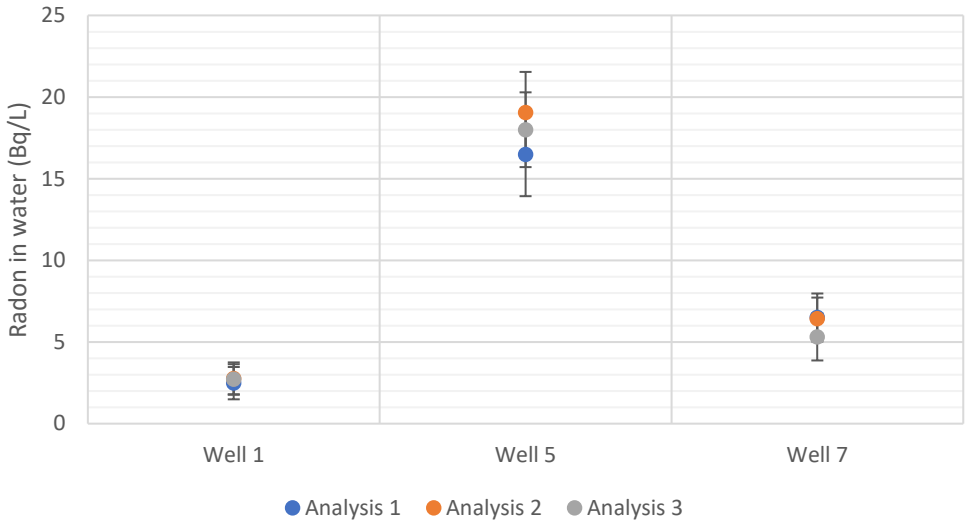

Figure 29 Radon concentrations for the Waikirikiri Selwyn groundwater samples.

4 Discussion

This chapter gives an overall discussion of the study's results and whether the aims of the study were achieved. The limitations of the study are also discussed, including future areas of research.

4.1 Grain Size Distribution

The first specific aim of this study was to use the sediment cores to determine grain size characteristics and lithology of the Waikirikiri Selwyn River braid plain. This was achieved by sieving the sample intervals and analysing the results.

There is considerable variability in the shape of the distribution curves for different sample intervals within and between different wells. This variability indicates that the gravels are heterogeneous in nature. The shape of the curves is influenced to some degree by the percentage of recovered sediment, with some sample intervals indicating the potential loss of the finer fractions. Core loss occurs when cobbles block the barrel of the 155 mm diameter drill bit. When the barrel becomes blocked by cobbles, a significant volume of water is needed for the drilling process, which results in the fines being washed away. While the grain size distribution data helps to conceptualise the subsurface of the area, the sampling limitations must be considered during any interpretation.

McLean (2018) argues that grain size distribution analysis can give unreliable results, due to its dependence on the amount of core recovery. It is important to note that the samples used for analysis are small in comparison to the scale of the study site and weighed ~1.0 to 3.5 kg. Also, the coring barrel of the drill bit is 115mm in diameter which is similar to or smaller than some of the pebbles encountered. Therefore, this grain size distribution

provides a reasonable approximation of the lithological variability of the study site under the limitations of data collection.

Analysis of the fines using the Lasersizer also affects the distribution curves as the results obtained are slightly different with each analysis due to the minute volume of sediment required. The Lasersizer only requires a few drops of the sediment mixed with the deflocculant; therefore, slightly different results could be produced every time an analysis is run. For example, <5 g of fine sediment from a total sample of 300 g is required for the analysis using the Lasersizer. Triplicates of the <63 μm sediment samples and the average result taken would have given greater certainty in these results in the distribution curves.

Due to the variability of sediment recovery from the five piezometers, it is difficult to directly compare the distribution curves and relate them to geological units. The piezometers installed to 16 m go through two different geological units which have been described by Brown and Wilson (1988). The upper geological unit comprises of grey stratified postglacial sandy gravels and thin silt lenses, known as the Springston Formation. The deeper unit is found at around 3– 5 m depth and consists of yellow-brown glacial outwash gravel, known as the Burnham Formation. The Burnham Formation is poorly– sorted, weakly– bedded silty gravel with some clay content and angular cobbles.

4.2 Hydraulic Conductivity Estimates

Three different formulae, Slichter, Kozeny –Carman and Beyer, were used to estimate the hydraulic conductivity from the grain size analysis with widely varying results. The variation in the hydraulic conductivity values calculated suggest that estimating hydraulic conductivity from grain size analysis is unsuitable for these types of gravels. The significant loss of fines in the drilling process, and loss of sediment structure with sieving, imply this is not a suitable

method for this substrate. Appendix A shows that the values calculated using the Slichter equation are consistently lower than the values calculated from the other formulae. This observation is supported by Cheng and Chen (2007) who suggested that the Slichter method is inaccurate in comparison to the other methods used. Cheng and Chen (2007) also noted that applying different hydraulic conductivity formulae to the same medium can give vastly different results, some of which may differ by a factor of 10 or 20, concurring with the results found in this study.

The hydraulic conductivity results show substantial variability vertically within each piezometer and across the study site, highlighting the heterogeneity of the area. This makes it difficult to extrapolate the results even on a reach scale (Brodie, 2007; Coluccio & Morgan, 2019) . It also shows that hydraulic conductivity can vary significantly even with small changes in sediment structure (Eggleston & Rojstaczer, 2001). The calculated hydraulic conductivity values which are greater than 1000 m / d are either physically unrealistic values for a sandy gravel, or are more representative of open framework gravels. Dann et al. (2008) used pump tests to measure hydraulic conductivity in the Central Plains Aquifer in Canterbury. They calculated an average conductivity of ~100 m / d, which is similar to values calculated in this study where there was 100% recovery. The conductivity of the higher permeability channels studied by Dann et al. (2008) were found to be ~8,200 m / d. The variability of the hydraulic conductivity within this study and also Dann et al. (2009) are unsurprising due to the heterogeneity of the subsurface.

Although the results from this study are similar to previous research there are still limitations and assumptions with these methods when relating grain size analysis to hydraulic conductivity. The loss of the sediment structure is considered to be the most

significant limitation when calculating hydraulic conductivity from grain size analysis (McLean, 2018). Therefore, the hydraulic conductivity values derived from the grain size analysis does not reflect the horizontal or vertical component of *K* (Cheng & Chen, 2007; Cheong et al., 2008; Coluccio & Morgan, 2019) .

4.3 Porosity and Bulk Density

The total porosity measured for the sediments from Selwyn 5 varies vertically from 0.18 to 0.25 and the calculated bulk densities range from 1599 to 1679 kg/m^3 as per sections 2.3 and 2.4. These results are consistent with Dann et al. (2009), who measured porosity and bulk density at four locations in the Canterbury Plains all within the Springston Formation. They calculated a porosity of 0.17 for sandy gravel sediments and the bulk density was in the range 2000 to 2330 kg/m^3. For open framework gravels they measured a total porosity of 0.34. Pang et al. (2005) used a study site at Burnham, Canterbury and applied the values of effective porosity measured by North Canterbury Catchment Board and Regional Water Board (NCCB & RWB, 1983). Porosity is calculated from the volume of the voids, whereas effective porosity is the porosity available for the water to flow through, that is through interconnected pores. The North Canterbury Catchment Board measured an effective porosity ranging between 0.1 and 0.3 for the poorly sorted alluvium gravels agreeing with the measured values of this study which range from 0.18 to 0.30.

The measured porosity in this study was dependent on how well the jars were packed and the percentage of sediment recovery, and therefore serves as an estimate. For a true in-situ porosity value, freeze coring may give a better representation (Coluccio & Morgan, 2019).

4.4 Radon

Determining the spatial variability of radon equilibrium concentrations of sediments was undertaken in this study. The radon concentration of varying grain size fractions and the evaluation of radon as a tracer in groundwater–surface water exchange was also investigated as per my second and third aim.

4.4.1 Radon Equilibrium Concentration

The results of this study, in the Waikirikiri Selwyn River, show there is a greater concentration of radon diffusing from the fine sediments. For example, the <63 µm grain size fraction has radon equilibrium concentrations ranging from 2.4 to 5.6 Bq/L, whereas the <500 µm sediments have radon concentrations ranging from 0.58 to 0.9 Bq/L. This is consistent with previous research showing that grain size influences how much radon emanates from a material (Chanyotha et al., 2014; Sakoda et al., 2011).

This is also supported by the observation of Barton and Ziemer (1986) who measured the radon emanation from coal ash and found that the radon concentration increased as the particle size decreased. Breitner et al.(2010) studied granitic esker sand and also found that the radon concentration increased from 50 Bq/kg for the 1 –2 mm grain size to 200 Bq/kg for the <63 µm grain size fraction. Both of these studies concur with the findings within this study that radon emanation increases as grain size decreases.

Radon emanation concentrations were calculated across the study site. These ranged from 0.28 to 7.6 Bq/kg for the different grain size fractions. Sakoda et al. (2011) investigated the variation of radon emanation from different rocks and minerals. This study shows that there can be a wide variation in radon emanation from different types of sands and gravels. For example, a gravelly sandy loam, from the U.S.A., had a measured radium concentration of

33 Bq/kg. The concentration of radon emanating will depend on the radium content of the rocks and soils and the distribution of radium within the sediments.

A comparison was undertaken between plastic and aluminium lids with glass jars in the radon equilibration emanation experiments. The results show there was no significant difference between the different lid types. From the results table in Appendix B, it is evident that a wide variety of vessels have been used for radon experiments. Previous research undertaken by Erlandson et al. (2001) observed that plastic bottles, even 1-mm thick, are shown to have a radon loss of 10% per day, therefore it is vital that glass bottles are used. Radon does not diffuse through metal. However, despite changing the lids from plastic to aluminium, the measured radon concentrations did not significantly increase, suggesting possible gas loss in the jars used. Further research is required to ensure the vessel used for the experiments has no gas loss while in storage.

4.4.2 Radon Emanation Rate Experiments and Experimental Set-up

The results presented for the radon equilibrium rate experiments, in Section 3.3.4, do not show any significant trend in radon concentration over time. This may be attributed to gas loss from the jars. The measured concentration in the 500 mL jars with plastic lids after 5 days ranges from 0.39 to 0.55 Bq/L. After 10 days this increased from 1.33 to 2.51 Bq/L. However, after 15 and 20 days the concentrations were 1.4 to 1.6 Bq/L and 0.94 to 1.33 Bq/L, respectively. If there was no gas loss in the jars the results should steadily increase as the radon reaches equilibrium. The error in the radon equilibrium concentration results must also be considered, as this is substantial, and may be masking the gradual increase in radon concentration after 10 days.

During the laboratory experiments it was noted that several jars had an air bubble, despite being sealed under water. However, this is not thought to have affected the results of the experiment because applying the Fritz Weigel equation (Schubert et al., 2012) shows the size of the air bubble relative to the jar used is insignificant.

Other factors that could cause the radon concentration in the water to decrease is when the jars are opened and the sample water extracted. Ongori et al. (2015) studied the transfer of radon to air at the water air interface at low turbulence and estimated the transfer velocity coefficient of radon. The radon transfer coefficient was found to be 1.4×10^{-6} m/s. This shows that the time taken to open the jars and extract the sample would have minimal impact on the results measured as the velocity of the transfer of radon from water to air is small.

4.4.3 Bentonite and Granite

A laboratory emanation test was carried out to determine if water interaction with bentonite clay could increase the radon concentration in groundwater. Bentonite is a mineral sorbent (Pusch, 2015). Therefore, if the water contacts the bentonite along its flow path it may alter the radon concentration in the groundwater. The bentonite granules returned a measured radon concentration of 0.47 to 1.05 Bq/L. This range is lower than expected, as bentonite is a clay from the smectite clay group which are an extremely fine group of clays (Pusch, 2015). Therefore, a result similar to the <63 µm grain size fraction of 3.5 to 5 Bq/L was expected. The results of this test are inconclusive, since low radon concentrations could be the result of either gas leakage from the jars, or a low radon emanation flux from the bentonite.

The radon concentration of the Karamea Batholith granite analysed in the laboratory test produced results of 0.63 to 1.73 Bq/L or 0.4 to 1.12 Bq/kg. In a review of radon emanation of rocks and minerals by Sakoda et al. (2011), granite from the U.S.A, of particle size 1,400 to 4,000 µm, was tested. They found the radon emanation fraction to be 31.42 Bq/kg, which is significantly higher than the granite tested in this study. The low result from this study from a known radioactive source concurs with the idea that there may be gas loss in the jars. However, it should be noted that different types of granite contain differing amounts of radon and it may be that New Zealand granite has considerably less radon than granite from elsewhere in the world. Sakoda et al. (2011) showed that granite from different areas of the U.S.A have differing radium concentrations. For example, a granite pebble had a radium concentration of 13 Bq/kg, whereas granite saprolite has a radium concentration of 65 to 110 Bq/kg. This suggests that the results from granite immersion tests are inconclusive.

4.4.4 Groundwater sampling

Close et al. (2014) sampled radon concentrations in groundwater near the Waimakariri River in Canterbury and measured values of 4.0 to 25.2 Bq/L. Similar research was undertaken by Close (2014) at the Wairau River in Marlborough. The calculated radon equilibrium concentrations for the Wairau range from 7.6 to 9.2 Bq/L. Comparing the results of the radon groundwater concentrations of the Waimakariri and Wairau River studies, with the measured radon concentrations in the Waikirikiri Selwyn River, the measured radon concentrations in Selwyn 5 and Selwyn 7 are within the range of the results measured from these studies. The groundwater samples taken from the Waikirikiri Selwyn piezometers 1, 5 and 7 range from 2.4 Bq/L in Selwyn 1; 19Bq/L in Selwyn 5 and 6.5Bq/L in Selwyn 7. However, it should be noted that during subsequent drilling of a nearby 30 m hole, the bentonite seal above the screen in Selwyn 1 became compromised. This was evident by a

change in water level and temperature in Selwyn 1 before and after drilling of the 30 m hole, indicating leakage of water down the casing. The construction integrity of this piezometer is now comprised and as a result the groundwater measured from this piezometer is a mixture of surface and groundwater, thus reducing the concentration of radon in the groundwater. Selwyn 1 was sampled after the drilling of the 30 m hole. Subsequent sampling of three shallow piezometers has been undertaken at the study site. The three shallow piezometers subsequently sampled are on the true right and are marked on Figure 1. Selwyn 24, a shallow piezometer, which is drilled to 5.5 m had a measured groundwater concentration of 4.0 to 5.6 Bq/L. The shallow production well, also drilled to 5.5 m had a radon concentration of 9.2 to 12.1 Bq/L and Reed 2, which was drilled to 7.58 m, had a measured radon concentration of 6.3 to 10.9 Bq/L. These measured values are within the range of values obtained in the Waimakariri and Wairau River studies (Close et al. (2014)).

4.4.5 Comparison of RAD7 and Liquid Scintillation Methods

Analysis of the water from the bulk sediment samples using liquid scintillation counting produced results ranging from 2.18 to 4.0 Bq/L. However, the sample where the measured radon concentration was 4.0 Bq/L, contained some sediment whereas the other two samples analysed had clear water. The radon concentrations analysed with the RAD7 for the same sample interval, produced results ranging from 1.1 to 1.8 Bq/L. This range of values is slightly lower than the range of values recorded for the liquid scintillation counting. However, the error on the radon concentrations from the water samples analysed with the RAD7 ranged from 0.59 to 0.74 Bq/L, putting the results from the RAD 7 within the same range as the liquid scintillation counting. The measured radon concentrations from the water samples analysed via the liquid scintillation counting method for the <63 µm fraction

samples ranged from 3.65 to 5.01 Bq/L, compared to 3.0 to 4.6 Bq/L for the RAD7. The range in error on the RAD7 results was from 1.0 to 1.2 Bq/L, putting the RAD 7 results within the same range as the liquid scintillation method results. Therefore, giving confidence there was no gas loss during sampling. This indicates that the low radon values from the laboratory experiments are likely to have occurred during storage.

4.4.6 Radon as a Tracer

The third specific aim was to evaluate the usefulness of radon as a tracer for quantifying groundwater–surface water interaction.

Analysis of the radon concentrations from the differing grain size fractions in this study shows that more radon emanates from the <63 μm grain size fraction, suggesting that an increased amount of this grain size fraction in a sample would emanate more radon. If there had been 100% core recovery throughout the study site this could lead to greater radon concentrations measured and give a clearer indication as to whether the radon concentration does indeed vary significantly throughout the study site and within the piezometers.

The consistency of the groundwater sampling results with other New Zealand studies suggests that radon is a useful tool. The radon equilibrium concentrations measured from the sediments should exceed the values measured in the groundwater samples, suggesting there may be gas loss from the jars.

According to Sakoda et al. (2011) radon emanation from sediments is dependent on a variety of factors including grain size and shape, inner and outer pore size, temperature, moisture content, radium distribution in the grains, atmospheric pressure, radiation damage and soil density. They also noted that the most significant factor that influences radon

emanation is the radium distribution and this assumes all the radium is distributed evenly with every grain. The concentration of radium within the sediments is an important factor that can affect the radon emanation from sediments (Chanyotha et al., 2014). If the sediments contain low quantities of radium the sample size used for the immersion experiments may need to be increased in order to obtain a true representation. This suggests that the radium concentration and mineralogy of the sediments may be worth investigating. The factors affecting radon emanation highlighted by Sakoda et al. (2011), shows there are many ways radon emanation can be influenced and further investigation into these is required.

5 Conclusions

This study has provided baseline data within the research site on the radon equilibrium concentrations both spatially and within differing grain size fractions. The results suggest that radon concentrations in groundwater will depend on the volume of silts and clays, therefore, using radon as a tracer for groundwater–surface water interactions may be more complex than first thought.

The grain size analysis revealed a variety of distribution curves showing a large range in grain size fractions. The hydraulic conductivity values that were calculated from the grain size distributions ranged from 86 to >1000 m/d. The values showed a large variation with depth across the major stratigraphic units and there was also large spatial variability. As a result of core loss during the drilling process there was some bias towards larger grain size fractions. The calculated porosity ranged from 0.18 to 0.3 and the bulk density values

ranged from 1400 kg/m^3 to 1700 kg/m^3, which were similar to studies from a nearby experimental field site at Burnham, Canterbury.

Water from laboratory immersion results from 318 core sediment samples, have been analysed for radon concentrations. The sediment samples were recovered from four piezometers. The radon concentrations measuredranged from 0.4 to 5.6 Bq/L. This study found that the radon concentration varied with differing grain size, specifically the <63 µm fraction, which contained significantly higher radon concentrations than the other grain size fractions sampled. The laboratory immersion results indicate that the radon concentration increases with depth within both the Springston and Burnham formations.

This study in the Waikirikiri Selwyn River has provided further insight into using radon as a tracer for quantifying groundwater recharge rates from the Waikirikiri Selwyn River. However, the amount of radon emanating from sediments is dependent on a variety of factors such as grain size and shape, radium distribution, mineralogy, and the configuration and density of the sediments. Only grain size has been considered in this study. More information is required about the other factors affecting radon emanation to fully evaluate the suitability of radon as a tracer for quantifying recharge rates in New Zealand braided river systems.

Further work

Further work is required to ensure there is no gas loss in the experimental set-up, to ensure the sediments reach equilibrium, and there is confidence in the results obtained. This could include changing the vessel used completely, or turning the jars upside down so the gas is not in contact with the lid. From the results in Section 3.3.2, we can see that there is a

definite variation of radon with grain size as the values obtained for the 'fines' are considerably greater than the other grain size fractions. As the results for the laboratory experiments show consistently low radon concentrations, it would be beneficial to know the mineralogy and the radium concentration of the sediments. The Burnham Formation contains more silts and clays than the Springston Formation. With full core recovery during drilling, it may become apparent if there is more finer sediment material in the Burnham Formation and therefore potential for higher radon within this unit. Radon emanation measurements from the deeper sediments below the Burnham Formation would also provide a useful comparison to determine if there are other sources of radon in this environment that may be contributing to the higher concentrations as were observed in some of the groundwater samples.

The variability in hydraulic conductivity results highlights the importance of the core sediment recovery from the wells for calculating hydraulic conductivity via grain size analysis. It may be useful to measure hydraulic conductivity via pump tests or slug tests and compare the values obtained to the values calculated from the grain size analysis. Previous research by Cheong et al. (2008) noted that the loss of sediment structure of the core samples meant the hydraulic conductivity values calculated from grain size analyses were less representative of the physical properties of the sediments than in-situ pumping tests. However, if there were full sediment recovery the hydraulic conductivity results would be considerably altered.

References

AcuÑA, V., & Tockner, K. (2009). Surface–subsurface water exchange rates along alluvial river reaches control the thermal patterns in an Alpine river network. *Freshwater Biology, 54*(2), 306-320. https://doi.org/10.1111/j.1365-2427.2008.02109.x

Avery, E., Bibby, R., Visser, A., Esser, B., Moran, J., & Lawrence Livermore National Lab, L. C. A. (2018). Quantification of groundwater discharge in a subalpine stream using radon-222. *Water (Switzerland), 10*(2), 100. https://doi.org/10.3390/w10020100

Barton, T. P., & Ziemer, P. L. (1986). The effects of particle size and moisture content on the emanation of Rn from coal ash. *Health physics (1958), 50*(5), 581. https://go.exlibris.link/ml8yMWk9

Bourke, S., Cook, P., Shanafield, M., Dogramaci, S., & Clark, J. (2014). Characterisation of hyporheic exchange in a losing stream using radon-222. *Journal of Hydrology, 519*, 94-105. https://doi.org/10.1016/j.jhydrol.2014.06.057

Bovolo, C. I., Parkin, G., & Sophocleous, M. (2009). Groundwater resources, climate and vulnerability. *Environmental research letters, 4*(3), 035001. https://doi.org/10.1088/1748-9326/4/3/035001

Breitner, D., Arvela, H., Hellmuth, K. H., & Renvall, T. (2010). Effect of moisture content on emanation at different grain size fractions – A pilot study on granitic esker sand sample. *Journal of Environmental Radioactivity, 101*(11), 1002-1006. https://doi.org/10.1016/j.jenvrad.2010.07.008

Brodie, R., Sundaram, B., Tottenham, R., Hostetler, S., Ransley, T. (2007). *An Overview of Tools for Assessing Groundwater-Surface Water Connectivity*. https://www.researchgate.net/profile/Baskaran-Sundaram/publication/266472444_An_Overview_of_Tools_for_Assessing_Groundwater-Surface_Water_Connectivity/links/55388abb0cf226723ab6306a/An-Overview-of-Tools-for-Assessing-Groundwater-Surface-Water-Connectivity.pdf

Brown, L. J., Wilson, D. D., Moar, N. T., & Mildenhall, D. C. (1988). Stratigraphy of the late Quaternary deposits of the northern Canterbury Plains, New Zealand. *New Zealand journal of geology and geophysics, 31*(3), 305-335. https://doi.org/10.1080/00288306.1988.10417779

Cartwright, I., & Hofmann, H. (2016). Using radon to understand parafluvial flows and the changing locations of groundwater inflows in the Avon River, southeast Australia. *Hydrology and Earth System Sciences, 20*(9), 3581-3600. https://doi.org/10.5194/hess-20-3581-2016

Cartwright, I., Hofmann, H., Gilfedder, B., & Smyth, B. (2014). Understanding parafluvial exchange and degassing to better quantify groundwater inflows using 222Rn: The King River,

southeast Australia. *Chemical Geology, 380*, 48-60. https://doi.org/10.1016/j.chemgeo.2014.04.009

Cecil, L. D., & Green, J. G. (2000). Radon-222. In P. G. Cook & A. Herczeg (Eds.), *Environmental Tracers in Subsurface Hydrology* (pp. 175-194). Springer.

Chanyotha, S., Kranrod, C., & Burnett, W. C. (2014). Assessing diffusive fluxes and pore water radon activities via a single automated experiment. *Journal of Radioanalytical and Nuclear Chemistry, 301*(2), 581-588. https://doi.org/10.1007/s10967-014-3157-3

Chanyotha, S., Kranrod, C., Kritsananuwat, R., Lane-Smith, D., & Burnett, W. C. (2016). Optimizing laboratory-based radon flux measurements for sediments. *Journal of Environmental Radioactivity, 158-159*, 47-55. https://doi.org/10.1016/j.jenvrad.2016.03.023

Cheng, C., & Chen, X. (2007). Evaluation of methods for determination of hydraulic properties in an aquifer–aquitard system hydrologically connected to a river. *Hydrogeology Journal, 15*(4), 669-678. https://doi.org/10.1007/s10040-006-0135-z

Cheong, J.-Y., Hamm, S.-Y., Kim, H.-S., Ko, E.-J., Yang, K., & Lee, J.-H. (2008). Estimating hydraulic conductivity using grain-size analyses, aquifer tests, and numerical modeling in a riverside alluvial system in South Korea. *Hydrogeology Journal, 16*(6), 1129-1143. https://doi.org/10.1007/s10040-008-0303-4

Close, M. (2014). *Analysis of radon data from the Wairau River and adjoining Wairau plains aquifer*.

Close, M., Matthews, M., Burbery, L., Abraham, P., & Scott, D. (2014). Use of radon to characterise surface water recharge to groundwater. *Journal of Hydrology, 53*(2), 113-125.

Coluccio, K. (2018). *A comparison of methods for estimating groundwater-surface water interactions in braided rivers* [Master's Thesis, University of Canterbury]. Christchurch, New Zealand. http://hdl.handle.net/10092/15390

Coluccio, K., & Morgan, L. (2019). A review of methods for measuring groundwater–surface water exchange in braided rivers. *Hydrology and Earth System Sciences, 23*(10), 4397-4417. https://doi.org/10.5194/hess-23-4397-2019

Cook, P. (2013). Estimating groundwater discharge to rivers from river chemistry surveys. *Hydrological Processes, 27*(25), 3694-3707. https://doi.org/10.1002/hyp.9493

Cook, P., Favreau, G., Dighton, J., & Tickell, S. (2003). Determining natural groundwater influx to a tropical river using radon, chlorofluorocarbons and ionic environmental tracers. *Journal of Hydrology, 277*(1), 74-88. https://doi.org/10.1016/S0022-1694(03)00087-8

Cook, P., Lamontagne, S., Berhane, D., & Clark, J. (2006). Quantifying groundwater discharge to Cockburn River, southeastern Australia, using dissolved gas tracers 222Rn and SF6. *Water Resources Research, 42*(10), W10411-n/a. https://doi.org/10.1029/2006WR004921

Corbett, D. R., Burnett, W. C., Cable, P. H., & Clark, S. B. (1998). A multiple approach to the determination of radon fluxes from sediments. *Journal of Radioanalytical and Nuclear Chemistry, 236*(1), 247-253. https://doi.org/10.1007/BF02386351

Dann, R., Close, M., Flintoft, M., Hector, R., Barlow, H., Thomas, S., & Francis, G. (2009). Characterization and estimation of hydraulic properties in an alluvial gravel vadose zone. *Vadose zone journal, 8*(3), 651-663. https://doi.org/10.2136/vzj2008.0174

Dann, R. L., Close, M. E., Pang, L., Flintoft, M. J., & Hector, R. P. (2008). Complementary use of tracer and pumping tests to characterize a heterogeneous channelized aquifer system in New Zealand. *Hydrogeology Journal, 16*(6), 1177-1191. https://doi.org/10.1007/s10040-008-0291-4

Durridge. (2020a). *RAD7 electronic radon detector user manual*. www.durridge.com

Durridge. (2020b). *RAD H2O Radon in Water accessory for the RAD7 User Manual*. www.durridge.com

Eggleston, J., & Rojstaczer, S. (2001). The value of grain-size hydraulic conductivity estimates: Comparison with high resolution in-situ field hydraulic conductivity. *Geophysical research letters, 28*(22), 4255-4258. https://doi.org/10.1029/2000GL012772

Erlandsson, B., Jakobsson, B., & Jönsson, G. (2001). Studies of the radon concentration in drinking water from the horst Söderåsen in Southern Sweden. *Journal of Environmental Radioactivity, 53*(2), 145-154. https://doi.org/10.1016/S0265-931X(00)00119-3

Freeze, R. A., & Cherry, J. A. (1979). *Groundwater*. Prentice Hall Inc.

Gurdak, J. J., McMahon, P. B., & Bruce, B. W. (2012). Vulnerability of groundwater quality to human activity and climate change variability, High Plains aquifer, USA. In H. M.-B. Treidel, J.L.; Gurdak, J.J. (Ed.), *Climate change effects on groundwater resources: A global synthesis of findings and recommendations* (pp. 145-168). CRC Press/Balkema.

Hoehn, E., & Von Gunten, H. (1989). Radon in groundwater: A tool to assess infiltration from surface waters to aquifers. *Water Resources Research, 25*(8), 1795-1803. https://doi.org/10.1029/WR025i008p01795

Kalbus, E., Reinstorf, F., & Schirmer, M. (2006). Measuring methods for groundwater - surface water interactions: A review. *Hydrology and Earth System Sciences, 10*(6), 873-887. https://doi.org/10.5194/hess-10-873-2006

Lamontagne, S., & Cook, P. G. (2007). Estimation of hyporheic water residence time in situ using 222Rn disequilibrium. *Limnology and Oceanography: Methods, 5*(11), 407-416. https://doi.org/10.4319/lom.2007.5.407

Larned, S., Hicks, D., Schmidt, J., Davey, A., Dey, K., Scarsbrook, M., Arscott, D., & Woods, R. (2008). The Selwyn River of New Zealand: A benchmark system for alluvial plain rivers. *River Research and Applications, 24*(1), 1-21. https://doi.org/10.1002/rra.1054

Martindale, H. (2015). *The use of radon and complementary hydrochemistry tracers for the identification of groundwater-surface water interaction in New Zealand* [Master's Thesis, Massey University].

Martindale, H., Morgenstern, U., Singh, R., & Stewart, B. (2016). Mapping groundwater-surface water interaction using radon-222 in gravel-bed rivers: a comparative study with differential flow gauging. *Journal of Hydrology (New Zealand), 55*(2), 121-134.

McCallum, J., Cook, P., Berhane, D., Rumpf, C., & McMahon, G. (2012). Quantifying groundwater flows to streams using differential flow gaugings and water chemistry. *Journal of Hydrology, 416*, 118-132. https://doi.org/10.1016/j.jhydrol.2011.11.040

McLean, L. (2018). *Hydrogeological investigation of the Christchurch city aquifer* University of Canterbury]. Christchurch, New Zealand.

Micrometrics. (2012). *Saturn Digisizer 5200*.

Moore, W. (1997). High fluxes of radium and barium from the mouth of the Ganges-Brahmaputra River during low river discharge suggest a large groundwater source. *Earth and Planetary Science Letters, 150*(1), 141-150. https://doi.org/10.1016/S0012-821X(97)00083-6

Mullinger, N. J., Pates, J. M., Binley, A. M., & Crook, N. P. (2009). Controls on the spatial and temporal variability of 222Rn in riparian groundwater in a lowland Chalk catchment. *Journal of hydrology (Amsterdam), 376*(1), 58-69. https://doi.org/10.1016/j.jhydrol.2009.07.015

Nazaroff, W. W. (1992). Radon transport from soil to air. *Reviews of geophysics (1985), 30*(2), 137-160. https://doi.org/10.1029/92RG00055

NCCB, & RWB. (1983). *Interim report on the Groundwater Resource of the Central Plains*.

Odong, J. (2007). Estimation of evaluation of empirical formulae for determination of hydraulic conductivity based on grain size analysis. *Journal of American Science, 3*, 54-60.

Ongori, J. N., Lindsay, R., & Mvelase, M. J. (2015). Radon transfer velocity at the water–air interface. *Applied Radiation and Isotopes, 105*, 144-149. https://doi.org/10.1016/j.apradiso.2015.07.058

Pang, L., Close, M., Goltz, M., Noonan, M., & Sinton, L. (2005). Filtration and transport of Bacillus subtilis spores and the F-RNA phage MS2 in a coarse alluvial gravel aquifer: Implications in the estimation of setback distances. *Journal of contaminant hydrology, 77*(3), 165-194. https://doi.org/10.1016/j.jconhyd.2004.12.006

Pusch, R. (2015). Nature of Smectites. In *Bentonite Clay*. CRC Press.

Rodgers, P., Soulsby, C., Petry, J., Malcolm, I., Gibbins, C., & Dunn, S. (2004). Groundwater–surface-water interactions in a braided river: a tracer-based assessment. *Hydrological Processes, 18*(7), 1315-1332. https://doi.org/10.1002/hyp.1404

Rupp, D., Larned, S., Arscott, D., & Schmidt, J. (2008). Reconstruction of a daily flow record along a hydrologically complex alluvial river. *Journal of Hydrology, 359*(1), 88-104. https://doi.org/10.1016/j.jhydrol.2008.06.019

Sadat-Noori, M., & Glamore, W. (2019). Porewater exchange drives trace metal, dissolved organic carbon and total dissolved nitrogen export from a temperate mangrove wetland. *Journal of environmental management, 248*, 109264. https://doi.org/10.1016/j.jenvman.2019.109264

Sakoda, A., Ishimori, Y., & Yamaoka, K. (2011). A comprehensive review of radon emanation measurements for mineral, rock, soil, mill tailing and fly ash. *Applied Radiation and Isotopes, 69*(10), 1422-1435. https://doi.org/10.1016/j.apradiso.2011.06.009

Schubert, M., Kopitz, J., & Chałupnik, S. (2014). Sample volume optimization for radon-in-water detection by liquid scintillation counting. *Journal of Environmental Radioactivity, 134*, 109-113. https://doi.org/10.1016/j.jenvrad.2014.03.005

Schubert, M., Paschke, A., Lieberman, E., & Burnett, W. C. (2012). Air–Water Partitioning of 222Rn and its Dependence on Water Temperature and Salinity. *Environmental science & technology, 46*(7), 3905-3911. https://doi.org/10.1021/es204680n

Stellato, L., Petrella, E., Terrasi, F., Belloni, P., Belli, M., Sansone, U., & Celico, F. (2008). Some limitations in using 222Rn to assess river–groundwater interactions: the case of Castel di Sangro alluvial plain (central Italy). *Hydrogeology Journal, 16*(4), 701-712. https://doi.org/10.1007/s10040-007-0263-0

Stellato, L., Terrasi, F., Marzaioli, F., Belli, M., Sansone, U., & Celico, F. (2013). Is 222Rn a suitable tracer of stream–groundwater interactions? A case study in central Italy. *Applied Geochemistry, 32*, 108-117. https://doi.org/10.1016/j.apgeochem.2012.08.022

Sun, H., & Semkow, T. (1998). Mobilization of thorium, radium and radon radionuclides in ground water by successive alpha-recoils. *Journal of Hydrology, 205*(1), 126-136. https://doi.org/10.1016/S0022-1694(97)00154-6

Treidel, H., Martin-Bordes, J. L., & Gurdak, J. J. (2012). *Climate change effects on groundwater resources: a global synthesis of findings and recommendations* (1st ed.). CRC Press/Balkema. https://doi.org/10.1201/b11611

Vincent, C. (2005). *Hydrogeology of the upper Selwyn catchment* [Master's Thesis, University of Canterbury]. http://hdl.handle.net/10092/1137

Wang, Z., Lee, J., & Melching, C. (2015). Sediment movement in alluvial rivers. In *River Dynamics and Integrated River Management* (pp. 265-336). Springer Berlin Heidelberg. https://doi.org/10.1007/978-3-642-25652-3_6

White, P. A. (2001). Groundwater Resources in New Zealand. In M. R. Rosen & P. A. White (Eds.), *Groundwaters of New Zealand* (pp. 45-76). New Zealand Hydrological Society Inc.

Wilson, D. (1973). The significance of geology in some current water resource problems, Canterbury plains, New Zealand. *Journal of Hydrology (New Zealand), 12*(2), 103-118.

Appendix A Table of Hydraulic Conductivity Calculations

Well	Sample depth interval (m)	d60 (mm)	d10 (mm)	$C_u = \frac{d_{60}}{d_{10}}$	Slichter (m/d)	Kozeny-Carmen (m/d)	Beyer (m/d)
1	2.57-3.84	16	1	16	11,111	25,125	75,660
1	4.4-4.76	20	2.8	7	160125	400,550	732,154
1	4.76-5.96	12	0.12	100	136	301	509
1	8.4-8.9	17	3.4	5	325,452	874,938	1170,253
1	10.52-11.1	3.2	0.095	34	86	190	535
1	13.2-13.56	17	0.5	34	2376	5262	14,766
1	15.08-15.8	12	0.12	100	136	301	509
3	0.95-1.4	4.1	0.1	41	94	209	550
3	5.6-5.96	9	0.2	45	378	837	2117
3	13.56-14.4	1.3	0.17	8	554	1365	2652
3	14.85-15.08	14	0.1	140	94	209	279
5	3-3.9	15	0.35	43	1158	2557	6610
5	4.05-6.0	9	0.13	69	159	353	734
5	6.0-7.5	9	0.11	82	114	252	475
5	7.8-10.5	13	0.25	52	590	1305	3110
5	14-15	7	0.1	70	94	209	432
7	12.5-13.5	14	0.16	88	242	535	981
9	1.5-2.0	35	5	7	520,128	1305,504	2345,760
9	6.85-7.5	20	4	5	450,455	1210,982	1619,724
9	8.4-9.0	30	8.4	4	2606,783	7543,653	7664,907

Appendix B Table of Previous Radon Studies, Including Equipment Used

Study	Vessel	Equipment	notes
Krupp et al. ,2017. Radon emanation coefficients of several minerals	Polyethylene vessel	Durridge RAD7	
Chanyotha et al.,2016. Optimizing laboratory-based radon flux measurements for sediments	Pyrex glass bottle	Durridge RAD7	
Sadat-Noori and Glamore, 2019. Porewater exchange drives trace metal, dissolved organic carbon and total dissolved nitrogen export from a temperate mangrove wetland	Gas-tight container, with radium free water. Water extracted and collected in 6L gas-tight plastic bottles.	RAD7	

Study	Vessel	Equipment	notes
Stringer & Burnett, 2004. Sample bottle design improvements for radon emanation analysis of natural waters	6l high density polyethylene, with screw on rubber cap	RAD7	This is for direct sampling of groundwater, big bottle analysis.
Chanyotha et al., 2014. Assessing diffusive fluxes and pore water radon activities via a single automated experiment	700ml wide mouth glass bottle with gas tight lid	RAD7	
Eaton et al.,1995. Standard methods for examination of water and wastewater. Chapter 7-28	Sample bottle – polyethylene with gas-tight glass stopcock	Liquid scintillation cell	
Baixeras, Erlandsson et al., 2001 Radon emanation from soil samples	Plastic can with kodak film LR 115-II lining	Alpha activity counter from the kodak film under a microscope	

Study	Vessel	Equipment	notes
Cranswick, Cook, Lamontage, 2014. Hyporheic zone exchange fluxes and residence times inferred from riverbed temperature and radon data	150ml glass jars with DI water	Liquid Scintillation	

Appendix C Radon Emanation Experiment Method

Radon Emanation Concentration Method

Experimental set-up

- Jars and lids are weighed, then 20ml of water added to bottom and weighed
- add sediment and weigh
- Fill remaining space with radon free water and seal under water to ensure there are no bubbles. Label jars with date, sample no, well no and depth. Place in a cold store to encourage radon to stay in the water and not move into air if there are any wee bubbles.

Purging (5 mins)

- Purge rad 7 and tubing, with no vial attached, while monitoring the humidity status in the RAD 7 window.

  To monitor the humidity press start, enter, status, enter, then press the right arrow 3 times Ensure you purge through the glass fritz and the humidity is below 6% before running the next sample.

Sampling

- Take a 40 ml vial
- Extract some DI water into syringe from a beaker and then tap syringe to ensure there are no air bubbles in the small piece of tubing attached to the syringe. Push out all the water
- Unscrew jar as quickly as possible

- Extract 40ml of sample water, slowly, then put slowly into 40ml vial.
- Attach to aerator. Make sure clamp is open.

Sample aeration (10 mins)

- Use manual setting on DRYSTIK, press enter for 5 min cycle, duty cycle 100%, solenoid disabled. Press ↵ after each step
- Adjust the clamp, shown below to ensure sample is aerating, but not too much that water is forced up the tubes.

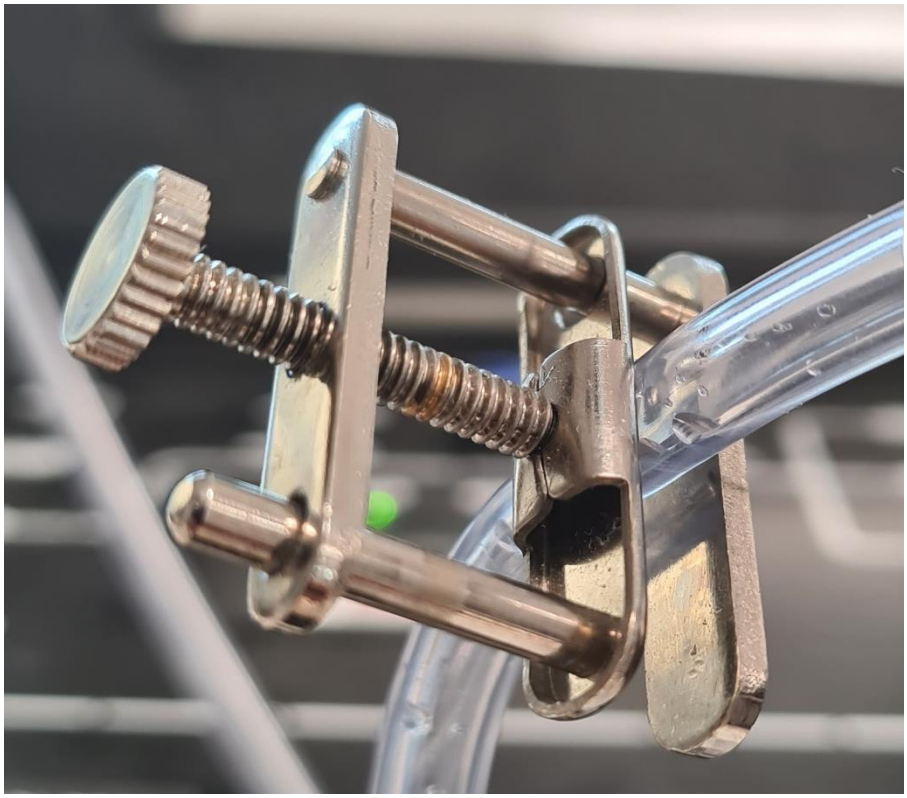

- Aerate for 10 mins, watch the bubbles as water can sometimes go up the tubes and the airflow may need to be adjusted using the clamp.

Counting

- Just before the sample as finished aerating start the test on the RAD7. Press menu, enter then ↓ until you get to start, then press enter

- On the DRYSTIK adjust the duty cycle to 30%. To do this press the enter key,  , then ↓ until you see duty cycle and use the ↑ and ↓ to adjust the %.
- Open the clamp so no bubbles are in the tube.
- Leave as is until the test has finished running.

End of test

- Once finished, remove sample, change the duty cycle to 100% and close the clamp so air is now flowing through the glass fritz. This is purging the equipment, do this for 5mins.
- Remove printout. Monitor humidity on RAD 7, press menu, enter, status then press the → twice to watch the humidity
- Once completed, switch off pump and get ready to test another sample. To switch off the pump press enter, then ↓until you see stop/exit and press enter.
- If humidity does not come down you may need to change the small tube of desiccant

Appendix D Radon Emanation Results

depth	grain size	Radon In Water [Bq/m3]	Radon In Water 2-Sigma Uncert. [Bq/m3]	Radon in water (Bq/l)	Radon in water 2-sigma uncertainty (Bq/l)	average vol of water	radon in vol of water (Bq/l)	radon in vol of water uncertainty (Bq/l)	average amount of sediment	radon in sediment (Bq/kg)	radon in sediment uncertainty (Bq/kg)
3.3.9	bulk	1400	380	1.4	0.38	0.2613	0.3658	0.0993	0.8322	0.44	0.1193
3.3.9	4	810	290	0.81	0.29	0.2810	0.2276	0.0815	0.8106	0.28	0.1005
3.3.9	2	590	250	0.59	0.25	0.0834	0.0492	0.0208	0.1147	0.43	0.1817
3-3.9	1	590	250	0.59	0.25	0.0935	0.0552	0.0234	0.0902	0.61	0.2592
3-3.9	0.5	900	300	0.9	0.3	0.0868	0.0781	0.0260	0.0997	0.78	0.2611
3-3.9	0.25	570	240	0.57	0.24	0.0925	0.0527	0.0222	0.0871	0.61	0.2549
3-3.9	0.125	680	270	0.68	0.27	0.0934	0.0635	0.0252	0.0876	0.72	0.2877
3-3.9	0.063	470	220	0.47	0.22	0.1026	0.0482	0.0226	0.0635	0.76	0.3555
3-3.9	<0.063	3490	610	3.49	0.61	0.0954	0.3328	0.0582	0.0717	4.64	0.8110
4.05-6.0	bulk	1880	440	1.88	0.44	0.2557	0.4807	0.1125	0.8407	0.57	0.1338
4.05-6.0	4	1870	440	1.87	0.44	0.2823	0.5279	0.1242	0.8101	0.65	0.1533
4.05-6.0	2	970	320	0.97	0.32	0.0852	0.0826	0.0273	0.1139	0.73	0.2394
4.05-6.0	1	590	250	0.59	0.25	0.0866	0.0511	0.0217	0.1062	0.48	0.2039
4.05-6.0	0.5	640	260	0.64	0.26	0.0922	0.0590	0.0240	0.0918	0.64	0.2611
4.05-6.0	0.25	990	320	0.99	0.32	0.0888	0.0879	0.0284	0.0972	0.90	0.2921
4.05-6.0	0.125	580	250	0.58	0.25	0.0919	0.0533	0.0230	0.0910	0.59	0.2525
4.05-6.0	0.063	630	260	0.63	0.26	0.0956	0.0602	0.0249	0.0803	0.75	0.3096
4.05-6.0	<0.063	2400	500	2.4	0.5	0.0949	0.2279	0.0475	0.0751	3.03	0.6320
6-7.5	bulk	1500	400	1.5	0.4	0.2821	0.4232	0.1129	0.7645	0.55	0.1476
6-7.5	4	1860	440	1.86	0.44	0.2872	0.5342	0.1264	0.7945	0.67	0.1591
6-7.5	2	1150	350	1.15	0.35	0.0822	0.0945	0.0288	0.1185	0.80	0.2429

depth	grain size	Radon In Water [Bq/m3]	Radon In Water 2-Sigma Uncert. [Bq/m3]	Radon in water (Bq/l)	Radon in water 2-sigma uncertainty (Bq/l)	average vol of water	radon in vol of water (Bq/l)	radon in vol of water uncertainty (Bq/l)	average amount of sediment	radon in sediment (Bq/kg)	radon in sediment uncertainty (Bq/kg)
6-7.5	1	800	290	0.8	0.29	0.0831	0.0665	0.0241	0.1151	0.58	0.2094
6-7.5	0.5	810	290	0.81	0.29	0.0876	0.0710	0.0254	0.1041	0.68	0.2441
6-7.5	0.25	520	230	0.52	0.23	0.0897	0.0467	0.0206	0.0984	0.47	0.2098
6-7.5	0.125	780	290	0.78	0.29	0.0882	0.0688	0.0256	0.0965	0.71	0.2653
6-7.5	0.063	500	170	0.5	0.17	0.0967	0.0484	0.0164	0.0771	0.63	0.2133
6-7.5	<0.063	3820	630	3.82	0.63	0.0940	0.3591	0.0592	0.0766	4.69	0.7728
7.8-10.5	bulk	1500	400	1.5	0.4	0.2792	0.4188	0.1117	0.7675	0.55	0.145514
7.8-10.5	4	1620	410	1.62	0.41	0.2804	0.4543	0.1150	0.8054	0.56	0.142762
7.8-10.5	2	240	160	0.24	0.16	0.0841	0.0202	0.0135	0.1147	0.18	0.1173
7.8-10.5	1	470	220	0.47	0.22	0.0865	0.0406	0.0190	0.1081	0.38	0.1759
7.8-10.5	0.5	730	280	0.73	0.28	0.0888	0.0648	0.0249	0.0985	0.66	0.2525
7.8-10.5	0.25	290	270	0.29	0.27	0.0947	0.0275	0.0256	0.0833	0.33	0.3069
7.8-10.5	0.125	600	250	0.6	0.25	0.1036	0.0622	0.0259	0.0616	1.01	0.4204
7.8-10.5	0.063	580	250	0.58	0.25	0.1045	0.0606	0.0261	0.0575	1.05	0.4543
7.8-10.5	<0.063	5620	770	5.62	0.77	0.0960	0.5397	0.0739	0.0736	7.33	1.0049
14-15	bulk	1840	440	1.84	0.44	0.2579	0.4745	0.1135	0.7995	0.59	0.1419
14-15	4	1040	330	1.04	0.33	0.2938	0.3055	0.0969	0.7705	0.40	0.1258
14-15	2	770	290	0.77	0.29	0.0862	0.0664	0.0250	0.1091	0.61	0.2293
14-15	1	520	230	0.52	0.23	0.0855	0.0445	0.0197	0.1097	0.41	0.1794
14-15	0.5	580	250	0.58	0.25	0.0927	0.0537	0.0232	0.0888	0.61	0.2608
14-15	0.25	730	280	0.73	0.28	0.0885	0.0646	0.0248	0.0983	0.66	0.2522
14-15	0.125	440	220	0.44	0.22	0.0947	0.0417	0.0208	0.0843	0.49	0.2472
14-15	0.063	400	200	0.4	0.2	0.1030	0.0412	0.0206	0.0629	0.65	0.3273
14-15	<0.063	4300	670	4.3	0.67	0.0897	0.3859	0.0601	0.0839	4.60	0.7168

Results of radon emanation from bulk samples across the study site, using jars with metal lids

Well	sample depth	Radon In Water [Bq/m3]	Radon In Water 2-Sigma Uncert. [Bq/m3]	Radon in water (Bq/l)	Radon in water 2-sigma uncertainty (Bq/l)	average vol of water	radon in vol of water (Bq/l)	radon in vol of water uncertainty (Bq/l)	average amount of sediment	radon in sediment (Bq/kg)	radon in sediment uncertainty (Bq/kg)
5	3.0-3.9	1400	380	1.4	0.38	0.261	0.366	0.099	0.832	0.440	0.119
5	4.05-6.0	1880	440	1.88	0.44	0.256	0.481	0.113	0.841	0.572	0.134
5	6.0-7.5	1500	400	1.5	0.4	0.282	0.423	0.113	0.764	0.554	0.148
5	7.8-10.5	1500	400	1.5	0.4	0.279	0.419	0.112	0.768	0.546	0.146
5	14-15	1840	440	1.84	0.44	0.258	0.474	0.113	0.799	0.593	0.142
1	2.57-3.84	1250	360	1.25	0.36	0.279	0.349	0.100	0.771	0.452	0.130
1	4.44-4.76	800	300	0.8	0.3	0.368	0.295	0.110	0.574	0.513	0.192
1	4.76-5.96	1490	390	1.49	0.39	0.319	0.475	0.124	0.680	0.698	0.183
1	8.4-8.9	600	250	0.6	0.25	0.273	0.164	0.068	0.833	0.196	0.082
1	10.52-11.1	980	320	0.98	0.32	0.314	0.308	0.100	0.686	0.449	0.146
1	13.2-13.56	1230	360	1.23	0.36	0.317	0.390	0.114	0.700	0.557	0.163
1	15.08-15.8	1370	380	1.37	0.38	0.317	0.435	0.121	0.690	0.630	0.175
3	0.95-1.4	760	280	0.76	0.28	0.324	0.246	0.091	0.670	0.367	0.135
3	5.6-5.96	1280	370	1.28	0.37	0.334	0.428	0.124	0.656	0.652	0.188
3	13.56-14.4	630	260	0.63	0.26	0.275	0.173	0.072	0.810	0.214	0.088
3	14.85-15.08	1010	330	1.01	0.33	0.326	0.329	0.108	0.660	0.499	0.163
7	12.5-13.5	1230	360	1.23	0.36	0.317	0.390	0.114	0.693	0.563	0.165

Results of radon emanation from Selwyn 5 for different grain size fractions for jars with plastic lids

well	sample depth	grain size	Radon In Water [Bq/m3]	Radon In Water 2-Sigma Uncert. [Bq/m3]	Radon in water (Bq/l)	Radon in water 2-sigma uncertainty (Bq/l)	average vol of water	radon in vol of water (Bq/l)	radon in vol of water uncertainty (Bq/l)	average amount of sediment	radon in sediment (Bq/kg)	radon in sediment uncertainty (Bq/kg)
5	3-3.9	2	650	260	0.65	0.26	0.0849	0.055185	0.022074	0.113	0.488363	0.195345
5	4.05-6.0	2	870	310	0.87	0.31	0.0864333	0.075197	0.02679433	0.1089	0.690514	0.246045
5	6.0-7.5	2	1040	340	1.04	0.34	0.0805	0.08372	0.02737	0.125833	0.665325	0.21751
5	7.8-10.5	2	570	240	0.57	0.24	0.0872	0.049704	0.020928	0.108833	0.456698	0.192294
5	14-15	2	490	230	0.49	0.23	0.0894	0.043806	0.020562	0.102267	0.428351	0.201063
5	3-3.9	1	830	290	0.83	0.29	0.0936	0.077688	0.027144	0.092067	0.843823	0.29483
5	4.05-6.0	1	740	350	0.74	0.35	0.0878	0.064972	0.03073	0.105933	0.613329	0.290088
5	6.0-7.5	1	780	280	0.78	0.28	0.0918	0.071604	0.025704	0.095233	0.75188	0.269905
5	7.8-10.5	1	680	270	0.68	0.27	0.0888667	0.060429	0.023994	0.1023	0.590707	0.234545
5	14-15	1	400	200	0.4	0.2	0.0901667	0.036067	0.01803333	0.100933	0.357332	0.178666
5	3.0-3.9	500	1050	330	1.05	0.33	0.0856667	0.08995	0.02827	0.1117	0.805282	0.253089
5	4.05-6.0	500	810	290	0.81	0.29	0.0863333	0.06993	0.02503667	0.109867	0.636499	0.227882
5	6.0-7.5	500	600	250	0.6	0.25	0.0995667	0.05974	0.02489167	0.074067	0.806571	0.336071
5	7.8-10.5	500	620	250	0.62	0.25	0.0874	0.054188	0.02185	0.106367	0.509445	0.205421
5	14-15	500	440	220	0.44	0.22	0.0929667	0.040905	0.02045267	0.092167	0.443819	0.22191
5	3.0-3.9	250	760	280	0.76	0.28	0.0914267	0.069484	0.02559947	0.096	0.723794	0.266661
5	4.05-6.0	250	900	310	0.9	0.31	0.0877	0.07893	0.027187	0.106167	0.743454	0.256078
5	6.0-7.5	250	930	310	0.93	0.31	0.0967667	0.089993	0.02999767	0.080767	1.114234	0.371411
5	7.8-10.5	250	690	270	0.69	0.27	0.0959333	0.066194	0.025902	0.083033	0.797198	0.311947
5	14-15	250	480	230	0.48	0.23	0.0972667	0.046688	0.02237133	0.081333	0.574033	0.275057
5	3.0-3.9	125	760	280	0.76	0.28	0.0878767	0.066786	0.02460547	0.1069	0.624755	0.230173
5	4.05-6.0	125	500	230	0.5	0.23	0.0892	0.0446	0.020516	0.1069	0.417212	0.191918
5	6.0-7.5	125	750	280	0.75	0.28	0.0953333	0.0715	0.02669333	0.0827	0.864571	0.322773
5	7.8-10.5	125	500	230	0.5	0.23	0.1011	0.05055	0.023253	0.069667	0.725598	0.333775
5	14-15	125	630	260	0.63	0.26	0.09352	0.058918	0.0243152	0.088267	0.667495	0.275474

well	sample depth	grain size	Radon In Water [Bq/m3]	Radon In Water 2-Sigma Uncert. [Bq/m3]	Radon in water (Bq/l)	Radon in water 2-sigma uncertainty (Bq/l)	average vol of water	radon in vol of water (Bq/l)	radon in vol of water uncertainty (Bq/l)	average amount of sediment	radon in sediment (Bq/kg)	radon in sediment uncertainty (Bq/kg)
5	3.0-3.9	63	740	280	0.74	0.28	0.1030333	0.076245	0.02884933	0.0644	1.183923	0.447971
5	4.05-6.0	63	900	300	0.9	0.3	0.0964	0.08676	0.02892	0.081433	1.065411	0.355137
5	6.0-7.5	63	520	230	0.52	0.23	0.0814333	0.042345	0.01872967	0.055333	0.765277	0.338488
5	7.8-10.5	63	520	230	0.52	0.23	0.1049333	0.054565	0.02413467	0.057867	0.942949	0.417074
5	14-15	63	510	230	0.51	0.23	0.1027267	0.052391	0.02362713	0.063133	0.829841	0.374242
5	3.0-3.9	<63	4260	670	4.26	0.67	0.096	0.40896	0.06432	0.0752	5.438298	0.855319
5	4.05-6.0	<63	3560	680	3.56	0.68	0.0875667	0.311737	0.05954533	0.095833	3.252911	0.621343
5	6.0-7.5	<63	3770	630	3.77	0.63	0.1017333	0.383535	0.064092	0.0605	6.339416	1.059372
5	7.8-10.5	<63	4600	700	4.6	0.7	0.1038333	0.477633	0.07268333	0.056667	8.428824	1.282647
5	14-15	<63	3660	620	3.66	0.62	0.0967667	0.354166	0.05999533	0.0726	4.87832	0.826382

Appendix E Raw RAD7 Data

Each run was downloaded into a folder. An example of the files is shown in Figure 30 below. The files are named by the run number, the grain size and the sample number. The sample number matches to the original excel spreadsheet used.

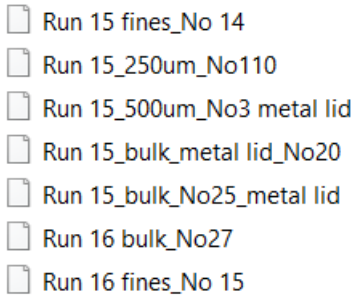

Figure 30 Example of files downloaded from RAD7

Once triplicates of each grain size were completed the runs were combined using the Capture software. Figure 31 shows an example of the combined files. The files were named by the well, then the sample interval, the grain size and then if the jar had a metal or plastic lid. All these files are stored on my UC computer, with backups on my laptop and an external hard drive.

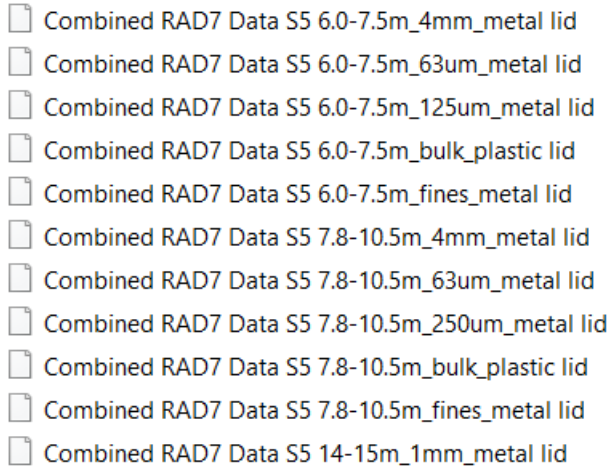

Figure 31 Example of files with combined data